The Dynamical Simulation of the Community Atmosphere Model Version 3 (CAM3)

JAMES W. HURRELL, JAMES J. HACK, ADAM S. PHILLIPS, JULIE CARON, AND JEFFREY YIN

National Center for Atmospheric Research, Boulder, Colorado

(Manuscript received 22 February 2005, in final form 13 September 2005)

ABSTRACT

The dynamical simulation of the latest version of the Community Atmosphere Model (CAM3) is examined, including the seasonal variation of its mean state and its interannual variability. An ensemble of integrations forced with observed monthly varying sea surface temperatures and sea ice concentrations is compared to coexisting observations. The most significant differences from the previous version of the model [Community Climate Model version 3 (CCM3)] are associated with changes to the parameterized physics package. Results show that these changes have resulted in a modest improvement in the overall simulated climate; however, CAM3 continues to share many of the same biases exhibited by CCM3.

At sea level, CAM3 reproduces the basic observed patterns of the pressure field. Simulated surface pressures are higher than observed over the subtropics, however, an error consistent with an easterly bias in the simulated trade winds and low-latitude surface wind stress. The largest regional differences over the Northern Hemisphere (NH) occur where the simulated highs over the eastern Pacific and Atlantic Oceans are too strong during boreal winter, and erroneously low pressures at higher latitudes are most notable over Europe and Eurasia. Over the Southern Hemisphere (SH), the circumpolar Antarctic trough is too deep throughout the year.

The zonal wind structure in CAM3 is close to that observed, although the middle-latitude westerlies are too strong in both hemispheres throughout the year, consistent with errors in the simulated pressure field and the transient momentum fluxes. The observed patterns and magnitudes of upper-level divergent outflow are also well simulated by CAM3, a finding consistent with an improved and overall realistic simulation of tropical precipitation. There is, however, a tendency for the tropical precipitation maxima to remain in the NH throughout the year, while precipitation tends to be less than indicated by satellite estimates along the equator.

The CAM3 simulation of tropical intraseasonal variability is quite poor. In contrast, observed changes in tropical and subtropical precipitation and the atmospheric circulation changes associated with tropical interannual variability are well simulated. Similarly, principal modes of extratropical variability bear considerable resemblance to those observed, although biases in the mean state degrade the simulated structure of the leading mode of NH atmospheric variability.

1. Introduction

Many studies have used the Community Atmosphere Model (CAM) and its predecessor, the Community Climate Model (CCM), to investigate the behavior of the earth's climate system. The CAM is a three-dimensional global atmospheric general circulation model (AGCM). The latest version (CAM3) was made available to the scientific community in June 2004. Moreover, CAM3 is a central component of the most recent version of the Community Climate System Model version 3 (CCSM3), which is a fully coupled global climate model also available for community use. In addition to CAM3, the CCSM3 includes component models for the ocean, land, and sea ice connected by a flux coupler (Collins et al. 2006a).

The purpose of this paper is to document the climatological behavior of the configuration of CAM3 used in simulations with CCSM3 for the upcoming Fourth Assessment Report (AR4) of the Intergovernmental Panel on Climate Change (IPCC). Results from a five-member ensemble of integrations forced by the observed global monthly varying mean sea surface temperatures (SSTs) and sea ice concentrations (SICs) are compared to contemporaneous observations. The em-

Corresponding author address: James W. Hurrell, National Center for Atmospheric Research, Climate and Global Dynamics Division, P.O. Box 3000, Boulder, CO 80307-3000.
E-mail: jhurrell@ucar.edu

TABLE 1. Characteristics of the CCM, the CAM, and the CCSM simulations used in this study. Details of each model can be found in the listed references.

Model	Reference	Resolution	Ocean	Averaging period
CCM3	Kiehl et al. (1998)	T42 L18	Prescribed	12 × (1979–2000)
CAM3	Collins et al. (2004, 2006b)	T85 L26	Prescribed	5 × (1979–2000)
CCSM3	Collins et al. (2005a)	T85 L26	Interactive dynamical ocean	100-yr control

phasis is on the dynamical representation of the model, including the seasonal variation of its mean state and aspects of its intraseasonal and interannual variability. Hack et al. (2006a) present features of the thermodynamic structure of CAM3, while those authors with Rasch et al. (2006) describe in detail the mean state and transient behavior of the simulated hydrological cycle. Collins et al. (2006b) present an overview of the model's radiative budget.

The outline of the paper is as follows. Brief descriptions of CAM3 and the validation data are presented in the next two sections. The general features of the simulated mean pressure, wind, and precipitation fields are given in section 4, including some comparisons to a widely used previous version of the model (CCM3) and to the fully coupled CCSM3 (Table 1). The representation of leading modes of atmospheric variability in CAM3, as well as its response to the El Niño–Southern Oscillation (ENSO) phenomenon, is also presented in section 4. The paper concludes with a summary of the primary simulation strengths and deficiencies of CAM3.

2. Overview of CAM3

The National Center for Atmospheric Research (NCAR) CAM3 is a global AGCM designed to produce simulations with good fidelity for several different dynamical cores and horizontal resolutions. The formulation of the physics and dynamics of CAM3 is detailed by Collins et al. (2004, 2006b). The standard version, used here, has 26 vertical levels and an 85-wave triangular spectral truncation (T85L26). A spectral Eulerian formulation provides the default treatment for resolved dynamical motions along with a semi-Lagrangian transport scheme for dealing with large-scale transport of water and chemical species. Most aspects of the dynamical core are identical to what was employed in CCM3 (Kiehl et al. 1998), although there are a number of changes (Collins et al. 2006b). The most important differences from CCM3 are associated with changes to the parameterized physics package. The representation of cloud and precipitation processes has been significantly revised (Boville et al. 2006), as have the treatments of aerosols and the parameterizations of radiation (Collins et al. 2006b). The CAM3 also includes the Community Land Model (CLM) version 3.0 for the treatment of land surface energy exchanges. The CLM3 is integrated on the same horizontal grid as CAM3, although each grid box is further divided into a hierarchy of land units, ground cover, and plant types (Oleson et al. 2004).

Relative to previous CCM versions, surface forcing more accurately considers the effects of fractional coverage by land and sea ice. Stand-alone integrations with CAM3 employ a new global SST and SIC dataset similar to that utilized by the European Centre for Medium-Range Weather Forecasts (ECMWF; see Fiorino 2004) in their 40-yr reanalysis project (ERA-40). This new dataset, to be described in a forthcoming manuscript, blends the monthly mean Hadley Center sea ice and SST dataset version 1 (HadISST1; Rayner et al. 2003) with version 2 of the National Oceanic and Atmospheric Administration (NOAA) weekly optimum interpolation (OI.v2) SST analysis (Reynolds et al. 2002). HadISST1 is used to supply ocean surface information prior to 1982, while OI.v2 is used thereafter. Both of these source datasets employ the same SIC–SST relationship in marginal sea ice zones. The only special processing of the source data for the CAM3 integrations included application of the midmonth calculation scheme of Taylor et al. (2000) to ensure that the monthly mean of the daily interpolated data was identical to the input monthly mean, and some subjective processing to support a smoother transition between the HadISST1 and OI.v2 products as well as to eliminate some SIC data that were judged to be spurious.

3. Validation data

Many different fields are examined in an attempt to gain a fairly complete view of the dynamical simulation, although more than can be presented here are available online at http://www.ccsm.ucar.edu/models/atm-cam/sims/cam3.0/. The primary source of validation data is the ERA-40 archive (see http://www.ecmwf.int/publications and http://www.ecmwf.int/research/era). In particular, we mostly make use of monthly mean data

available on 23 pressure levels in the vertical and a 2.5° horizontal resolution, although some daily output is utilized as well. Seasonal-mean climatologies were constructed from this archive, and the results were regridded to T42 spectral resolution for comparison to the model-generated, pressure-interpolated fields. Estimates of seasonal-mean precipitation rates were taken from the Climate Prediction Center (CPC) Merged Analysis of Precipitation (CMAP), a global monthly precipitation dataset constructed from satellite estimates, gauge observations and numerical model output. As Xie and Arkin (1996) caution, the actual quality of this merged precipitation product depends highly on the uncertain error structures of the individual data sources, so comparisons to CAM3 should be viewed as qualitative, not quantitative.

4. Results

Most results are presented in two-panel figures for mean December–February (DJF) and June–August (JJA) simulated climates. The format is to present the data from CAM3 in the top panel and either observations or differences from observations (e.g., CAM3 minus ERA-40) in the lower panel. Results from uncoupled CCM3 simulations and/or from the fully coupled configuration of CCSM3 are either noted or presented when differences from CAM3 are notable.

The CAM3 results are from what has become the standard AGCM experimental protocol: that where the model is forced with the known global evolution of SST and SIC. Such integrations form the basis of the Atmospheric Model Intercomparison Project (AMIP; Gates et al. 1999), and therefore are commonly referred to as AMIP experiments. We utilize a 5- (12) member T85 (T42) ensemble of CAM3 (CCM3) AMIP integrations that cover the period 1950–2000, and for most plots the ensemble mean is presented and compared to ERA-40 but only over the satellite era (i.e., 1979–2000; Table 1). CCSM3 data are from 100 yr of data extracted from an extended (>600 yr) control simulation using a T85 grid for the atmosphere and land and a 1° grid for ocean and sea ice (the configuration used in the IPCC AR4 simulations). For the CAM3, CCM3, and CCSM3 simulations, concentrations of greenhouse gases were held constant at 1990 levels, and the model results were truncated to T42 for direct comparison to the observational and CCM3 products. This truncation to a coarser horizontal resolution does not affect the interpretation of any large-scale features described here. For a more detailed discussion of the sensitivity of the simulated CAM3 climate to model resolution, the reader is referred to Hack et al. (2006b), Yeager et al. (2006), and DeWeaver and Bitz (2006).

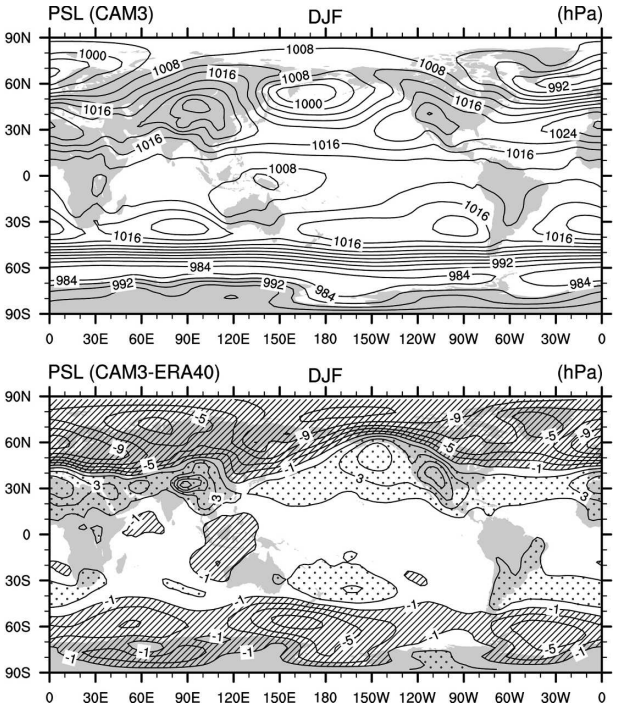

FIG. 1. (top) Mean DJF sea level pressure from CAM3 and (bottom) differences from the ERA-40 (1979–2000) climatology. The contour increment in the top panel is 4 hPa. Differences are contoured every 2 hPa from ±1 hPa, and positive (negative) differences are indicated by stippling (hatching).

a. Sea level pressure

The mean sea level pressure (SLP) pattern is a useful indication of an AGCM's ability to simulate the atmospheric circulation near the surface, and it represents an integrated measure of a model's thermodynamic and dynamic representations. The spatial distribution of the DJF and JJA means and differences from the ECMWF reanalyses are presented in Figs. 1 and 2. Because of the sea level reduction problem, differences over regions of high topography (e.g., the Himalayas, Greenland, the Andes, and Antarctica) are noisy and the magnitudes are not meaningful.

As for previous versions of the model (e.g., Hurrell et al. 1998), the CAM3 reproduces the main features of the observed SLP pattern quite well. This includes large interseasonal differences over the Northern Hemisphere (NH) related to the intensification of the subtropical high-pressure centers during northern summer and the high-latitude Aleutian and Icelandic low-pressure systems during boreal winter. The model also captures the largest seasonal pressure variations in the NH, which are found over the Asian continent and are related to the development of the Siberian anticyclone during winter and the monsoon low over Southeast

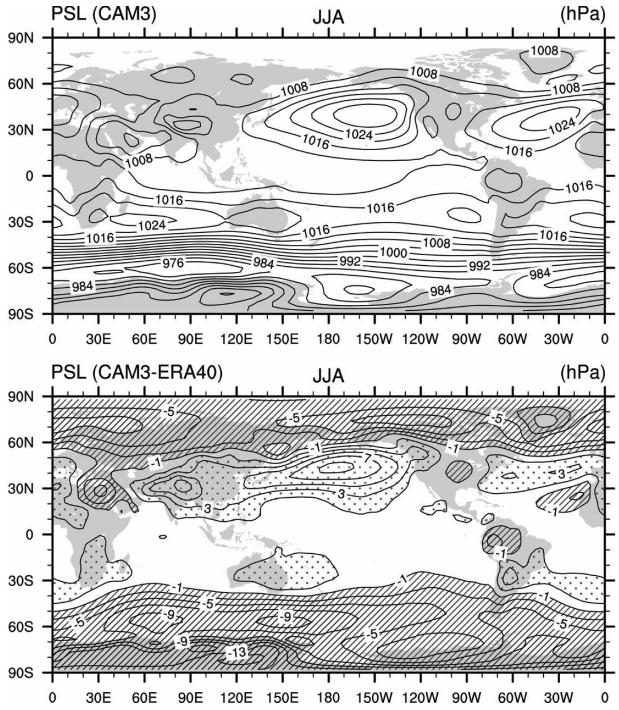

FIG. 2. As in Fig. 1 but for JJA.

Asia during summer. Over the Southern Hemisphere (SH), the SLP in CAM3 rises from the intertropical convergence zone (ITCZ) to a circumpolar peak in the subtropics where there is an anticyclone center in each ocean, in good agreement with observations. The subtropical belt of high pressure also lays a few degrees latitude farther poleward and is weaker during southern summer than winter in both the CAM3 and ERA-40, so that the oceanic subtropical highs over both hemispheres reach their peaks during JJA (Fig. 2). Farther poleward, the mean SLP rapidly drops to its lowest values in the circumpolar trough between 60° and 70°S. The zonally averaged pressure (not shown) in the circumpolar trough is about 4 hPa higher in southern summer than winter in the CAM3, again in good agreement with the observations.

Significant regional biases, however, are noticeable in the difference plots. Moreover, they are generally very similar in magnitude and position to those evident in CCM3 (Hurrell et al. 1998) and CCSM3 (not shown). During northern winter, SLP throughout the subtropics of both hemispheres is higher than observed: zonal mean differences are nearly 3 hPa (1.5 hPa) near 30°N (30°S). In contrast, simulated pressures are too low poleward of 50° latitude in both the NH and SH (Fig. 1), even a bit more so than in CCM3. Regionally, the Aleutian low does not extend as far east and south as observed, which contributes to a positive difference of more than 6 hPa over the eastern Pacific. This regional bias is not evident in CCSM3 (not shown), perhaps reflecting the importance of interactive SST effects over this region (Alexander et al. 2006) or differences in the distribution of tropical rainfall due to coupling (Hack et al. 2006a).

Over the northern Atlantic Ocean during DJF, the high-pressure ridge is too strong, especially over northern Africa, and differences of similar magnitude extend across the Middle East into Asia. The Icelandic low is also too deep, and it extends too far over Eurasia and the Arctic Basin relative to observations. This shortcoming, also evident in CCM3, results in erroneously low pressures (locally by −10 hPa and more) that extend across northern Europe well into Eurasia. Over the SH, the positions of the summertime subtropical ridges to the west of the continents are well represented, although shifted very slightly poleward. The model does better than CCM3 in capturing the observed asymmetries in the SH subtropical highs in which the pressure centers are shifted eastward toward the continents. The circumpolar Antarctic trough is well positioned, yet the central pressures are generally deeper than observed, resulting in a modestly stronger meridional gradient on the equatorward side of the trough. This bias is slightly larger in CCSM3 (not shown). Large (<−6 hPa) differences south of New Zealand are associated with the model's inadequate weakening and poleward shift of the maximum meridional pressure gradient over the Pacific. This notable and well-known feature of the SH climate (e.g., van Loon 1972) gives rise to the dominance of wavenumber 1 at middle and high latitudes (see also Fig. 5).

During southern winter (Fig. 2), the CAM3 SLP errors in high SH latitudes are larger than during summer and result from the circumpolar trough being too deep and too far equatorward, typical of earlier versions of the CCM as well (e.g., Hurrell et al. 1993, 1998). In particular, the zonal mean bias near 60°S is nearly −6 hPa (−10 hPa) in CAM3 (CCSM3). Although the model simulates a weakened meridional pressure gradient over the eastern Pacific, the observed changes are closer to the date line so again large differences from the atmospheric reanalyses are found south of New Zealand. Over the NH, the summer subtropical ridges over the Pacific and Atlantic in CAM3 are too strong and are shifted slightly poleward relative to observations. In particular, the central pressure of the Pacific high during JJA is near 1028 hPa in CAM3, compared to an observed value of 1024 hPa, and it is located nearly 5° latitude too far to the north resulting in a error exceeding 8 hPa locally. Similar errors in the central pressure and location are notable with the Azores

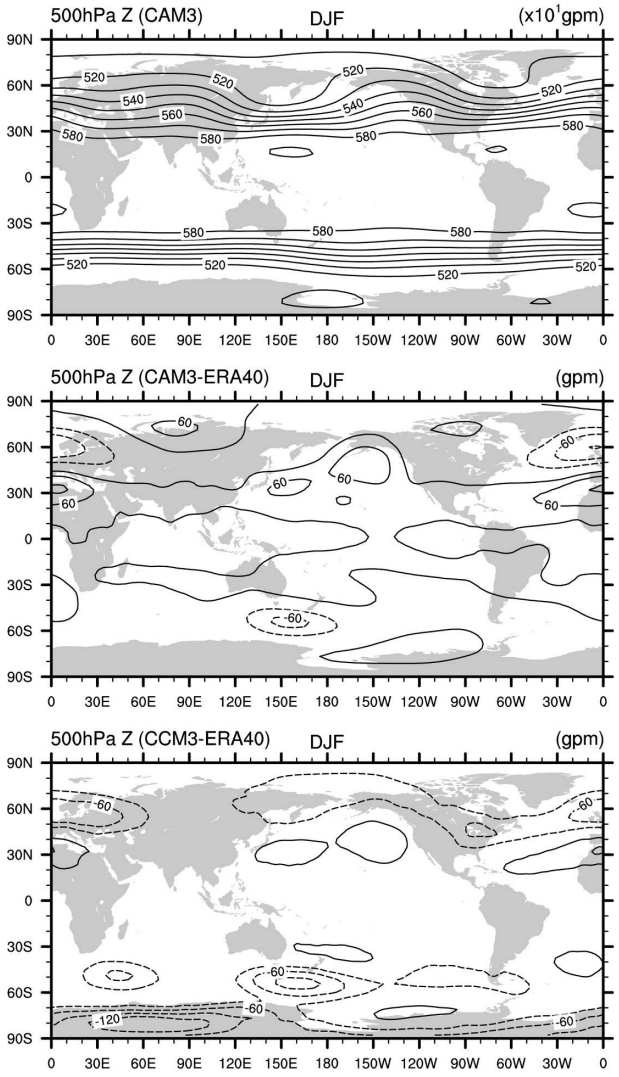

FIG. 3. (top) Mean DJF 500-hPa geopotential height from CAM3, differences from the ERA-40 (1979–2000) climatology for (middle) CAM3 and (bottom) CCM3. The contour increment in the top panel is 100 gpm. Differences are contoured every 30 gpm, negative values are dashed, and the zero contour is omitted.

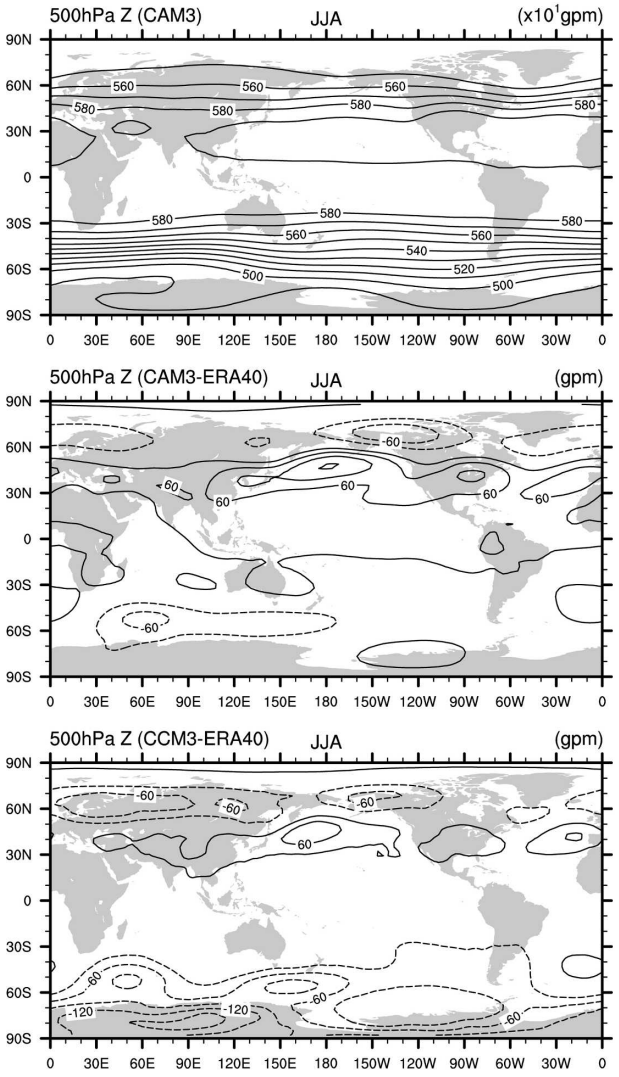

FIG. 4. As in Fig. 3 but for JJA.

high, although smaller than in the coupled model and improved over CCM3 (not shown).

b. Geopotential height

A climate parameter representative of the flow in the middle troposphere is the 500-hPa geopotential height field (Figs. 3 and 4). Many of the same characteristics seen in the SLP plots are evident at 500 hPa as well. Locally, CAM3 captures the major troughs off the east coasts of Asia and North America during northern winter, in addition to the trough over eastern Europe. The ridges over Russia, the west coast of North America, and the eastern Atlantic are also well simulated. Over the SH, as observed, the 500-hPa height gradient is weaker in the middle latitudes of the Pacific Ocean than in the same latitudes elsewhere during both seasons, which gives rise to a pattern of zonally asymmetric heights dominated by wavenumber 1 (e.g., Fig. 5). In the CAM3, as in the ERA-40 reanalyses, the locations of the zonal asymmetries in SH middle and high latitudes are the same in both seasons, but the amplitudes of the anomalies are larger during southern winter.

There are several differences from CCM3 of note (Figs. 3 and 4). In particular, simulated middle tropospheric heights at high latitudes of both hemispheres in CCM3 are lower than observed, consistent with a tropospheric cold bias in that model at extratropical latitudes (Hack et al. 1998). This widespread bias is not

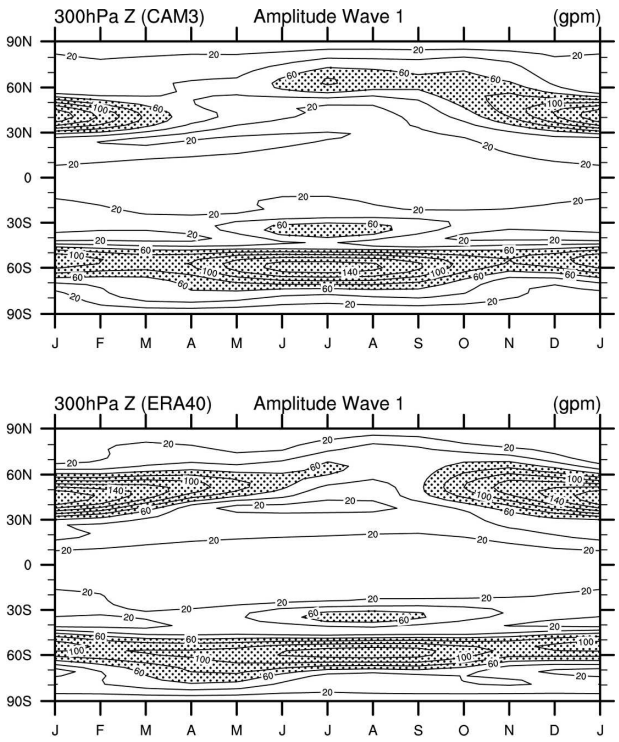

FIG. 5. The annual march of the amplitude of wavenumber 1 in 300-hPa geopotential heights from (top) CAM3 and (bottom) ERA-40. The contour increment is 20 gpm and values greater than 60 gpm are stippled.

evident in CAM3; however, higher than observed 500-hPa heights throughout the Tropics and subtropics in the new model were not a problem in CCM3. This low-latitude positive height bias is consistent with slightly warmer than observed temperatures throughout the tropical troposphere in CAM3 (Hack et al. 2006a), although in the tropical tropopause region warmer simulated temperatures are a notable improvement (Collins et al. 2006b).

Other regional differences from observations are largely consistent with the SLP biases discussed earlier. In particular, the ridge over the west coast of North America during DJF is shifted just to the west of the observed location at 500 hPa, resulting in an error of ~60 gpm over the Pacific, similar to the structure of the error in CCM3 but nearly twice the magnitude. The same bias is not evident in CCSM3, consistent with the improved simulation of the Aleutian low-pressure center in the coupled model (not shown). Over Europe, differences of −90 gpm reflect a simulated Atlantic ridge that does not extend as far to the east as observed and is too weak, while positive biases of the same magnitude over North Africa are significantly larger than in CCM3. The 500-hPa height biases over the SH are considerably smaller than in CCM3. The most notable differences from observed mean heights occur south of New Zealand, consistent with the largest SLP errors noted earlier.

Large-scale deviations from zonal means are described well by a Fourier decomposition of the geopotential heights along latitude circles. The annual cycles of the observed and CAM3 simulated amplitudes of wave 1 at 300 hPa are presented in Fig. 5. Over the SH, the amplitude of wave 1 reaches its peak during winter and early spring near 60°S in both the model and observations, although the simulated amplitudes are too large. The model also simulates the observed slight poleward movement of maximum amplitudes from southern summer into winter. More than 80% of the mean spatial variance is explained by wave 1 in DJF and JJA in CAM3, as in observations (not shown). Note that the CAM3 captures the observed second peak in the amplitude of wave 1 between 30° and 40°S, which is largest in southern winter.

The interseasonal changes in the quasi-stationary waves are largest over the NH, as captured by CAM3. Wave 1 has maximum amplitude of more than 160 gpm near 45°N during northern winter in the ERA-40 reanalyses. The maximum amplitude in CAM3 is smaller, although CCSM3 is closer to observations (not shown). The amplitude of wave 1 weakens from winter to summer, but it weakens too much in CAM3 in northern spring. In contrast to the SH, wave 1 during winter over the NH is baroclinic, leaning westward with height in both the model and observations (not shown), a feature evident in higher zonal harmonic waves as well. Another well-simulated feature not shown is that, near 30°N, wave 1 has peaks in the upper (near 150 hPa) and lower troposphere with a minimum near 500 hPa. Both the CAM3 simulated and observed phases reverse between the two peaks, reflecting the change in the monsoon over Asia from a low pressure center at sea level (Fig. 2) to a high pressure center in the upper troposphere. The monsoonal phase reversal with height is seen in waves 2 and 3 as well (not shown). All of these features are also characteristic of CCSM3, as they were for CCM3 (Raphael 1998; Hurrell et al. 1998).

c. Wind

The horizontal wind distribution is closely linked geostrophically to the temperature and pressure distributions. The zonal wind, in particular, has traditionally been one of the fundamental climate simulation verification parameters. Overall, the zonal wind structure is well simulated in CAM3 (Figs. 6 and 7), and the biases are very similar to those exhibited by CCM3 (Hurrell et al. 1998). The CAM3 simulated mean zonal flow in the

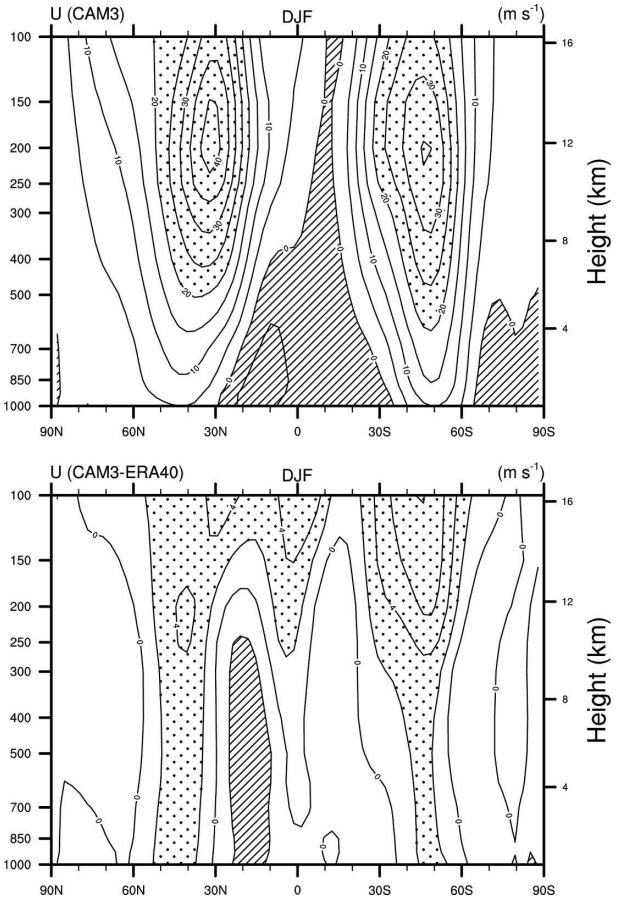

FIG. 6. (top) Zonally averaged mean DJF zonal wind from CAM3 and (bottom) differences from the ERA-40 (1979–2000) climatology. The contour increment in the top panel is 5 m s^{-1}, easterlies are hatched, and values greater than 20 m s^{-1} are stippled. Differences are contoured every 2 m s^{-1}, values less than -2 m s^{-1} are hatched, and differences greater than 2 m s^{-1} are stippled.

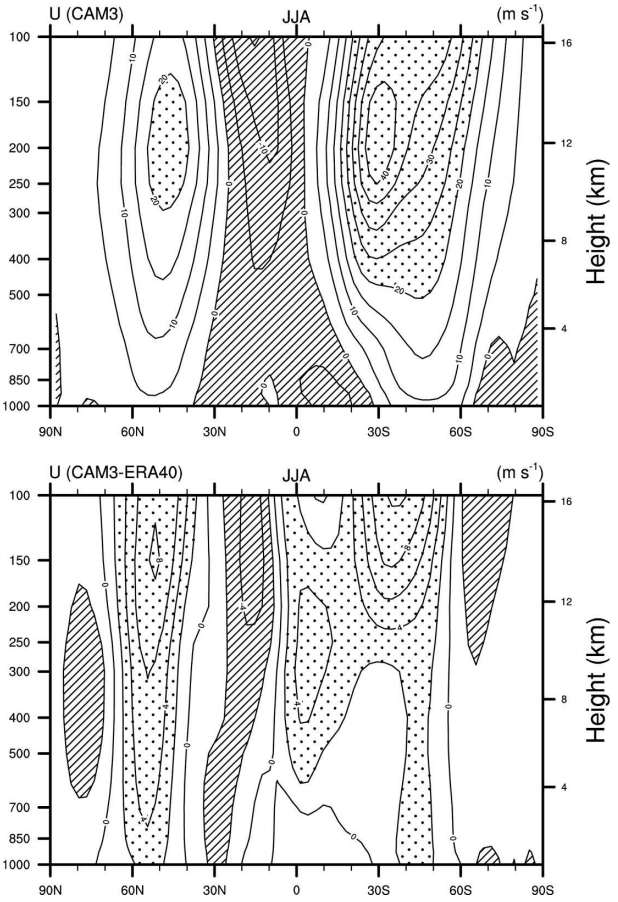

FIG. 7. As in Fig. 6 but for JJA.

NH during winter is very similar to the ECMWF winds, with the strongest westerlies more than 40 m s^{-1} near 200 hPa. Between 35° and 55°N, however, the zonally averaged westerlies in CAM3 are stronger than observed by a few meters per second, with a larger westerly bias evident during JJA. Over the SH, the simulated upper-tropospheric middle-latitude maximum during southern winter is about 2°–3° latitude nearer the equator than its NH winter counterpart, as observed. But in contrast to observations, it is stronger than the NH winter maximum by about 5 m s^{-1}, contributing to a relatively large upper-tropospheric westerly bias. This bias also reflects another shortcoming of the CAM3 SH winter simulation: the observed maximum near 30°S is clearly separated from a second westerly maximum in the upper troposphere that continues into the stratosphere, a feature not well captured by CCM3 either. A westerly bias is also evident at these latitudes and heights during southern summer.

In good agreement with observations, the simulated low-level easterlies are of nearly equal magnitude in each winter hemisphere and cover similar areas, and the upper-tropospheric tropical easterlies are much stronger in the NH than in the SH during summer. The summertime NH tropical easterlies in CAM3 are too strong (by ~4 m s^{-1}) and extend too far poleward, an aspect that was slightly better in CCM3 but worse in earlier versions of the CCM (Hurrell et al. 1993). Another persistent problem in earlier versions of the model was a westerly wind bias near the equator in the upper troposphere during both seasons. This error was considerably reduced in CCM3, and is even smaller in CAM3 although still in excess of 4 m s^{-1} during JJA (Fig. 7).

Regionally, in the upper troposphere, the strongest westerlies occur over the NH during winter (Fig. 8) and reach more than 70 m s^{-1} off the Asian coast and 40 m s^{-1} over the eastern United States and the western Atlantic. Westerlies extend across the equator over the

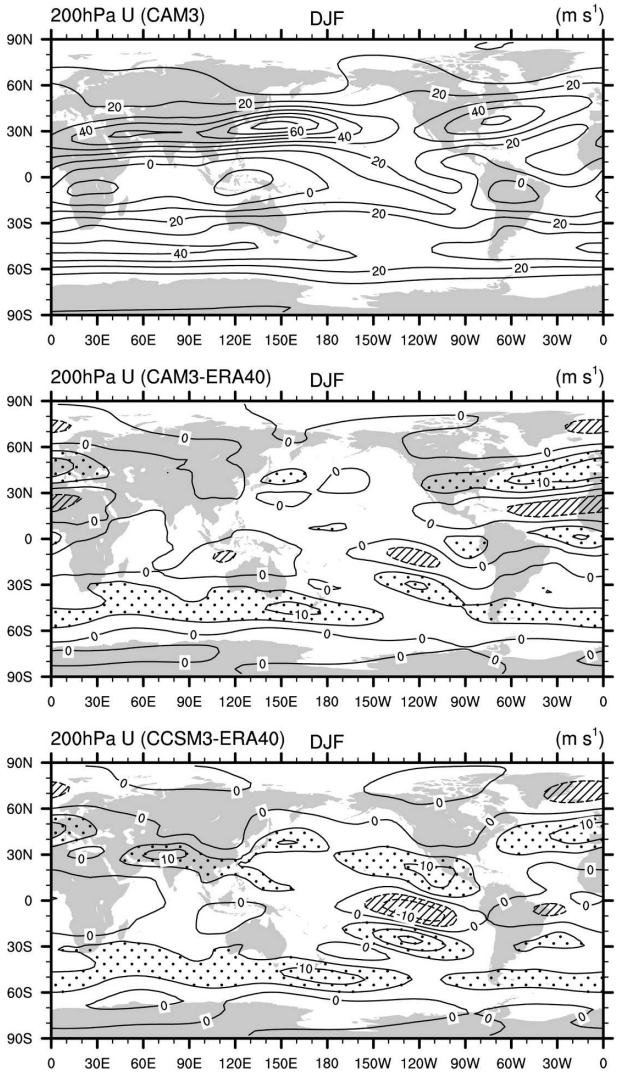

FIG. 8. (top) Mean DJF 200-hPa zonal wind from CAM3, (middle) differences from the ERA-40 (1979–2000) climatology for CAM3, and (bottom) CCSM3. The contour increment in the top panel is 10 m s^{-1}. Differences are contoured every 5 m s^{-1}, values less than -5 m s^{-1} are hatched, and differences greater than 5 m s^{-1} are stippled.

Atlantic and central Pacific Oceans during northern winter, and over the SH the peak in the westerlies is reached between 40° and 50°S with maxima more than 30 m s^{-1} over the Atlantic and Indian Oceans. All of these mean features are well simulated in CAM3, although the jet over the North Atlantic is too strong and extends too far to the southeast resulting in a westerly bias of more than 10 m s^{-1} over Europe, roughly twice that evident in CCM3 (not shown). A bias of similar magnitude is evident south of Australia extending east across New Zealand, and the new model overestimates the strength of the SH westerlies throughout this latitude band, as did CCM3. Very similar errors are evident throughout the SH in CCSM3 during southern summer (Fig. 8), but differences from the uncoupled CAM3 simulation are notable elsewhere. In particular, the East Asian westerly maximum is stronger in CCSM3 and exceeds that observed by more than 10 m s^{-1}, although the westerly bias across the North Atlantic is less than in CAM3. There is also a large (<-10 m s^{-1}) easterly bias just south of the equator near 125°W in CCSM3, flanked in the subtropics of both hemispheres by strong westerly biases. These features are also evident in CAM3, although they are considerably smaller in magnitude. Over the tropical North Atlantic, the large westerly bias in CAM3 is not evident in the coupled simulation, nor is the easterly bias over the subtropics.

During northern summer at 200 hPa several notable features of the simulation are again in good agreement with the observations (Fig. 9). A closed circulation is evident over the southern part of Asia, accompanied by a northward shift and substantial weakening of the higher-latitude westerly jet stream, although in both CAM3 and CCSM3 the simulated shift is too far poleward and the westerly maxima too strong. This results in a westerly error in the zonal average near 50°N (Fig. 7). Tropical easterlies encircle the near-equatorial latitudes in CAM3 and are strongest over Africa and the Indian Ocean with peak values near -20 m s^{-1} (the tropical easterly jet), generally conforming to observations. However, the simulated easterlies are too strong and are too far north and west over the subtropical North Atlantic and North Africa, producing a westerly error centered near the equator and an easterly error to the north, as was noted for CCM3 (Hurrell et al. 1998). The CAM3 easterlies also do not extend as far south as observed over the tropical Indian and western Pacific Oceans, contributing to a westerly bias that is even more pronounced in CCSM3 (Fig. 9). In contrast to CAM3, the fully coupled model also fails to simulate the observed easterlies near the equator over the eastern Pacific and South America, yielding a westerly bias in excess of 20 m s^{-1}.

A striking feature of the wintertime 200-hPa zonal winds over the SH is a maximum near 30°S with values near 50 m s^{-1} over Australia and the Pacific, a feature also evident in CAM3 (Fig. 9). The strongest westerlies extend too far west and south over the Indian Ocean, however, and the simulated 200-hPa westerlies near 40°S are about 10 m s^{-1} stronger on average than the ERA-40. Notwithstanding this bias, both the CAM3 and the CCSM3 successfully reproduce the observed spiraling of the maximum westerlies over the Indian Ocean through the middle latitudes to higher latitudes

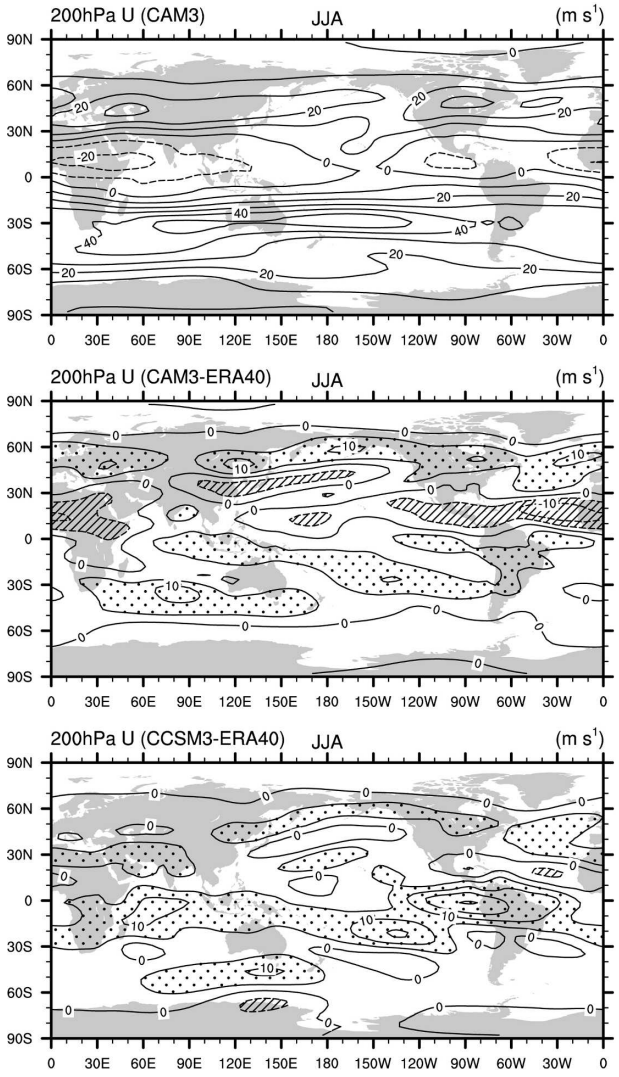

FIG. 9. As in Fig. 8 but for JJA.

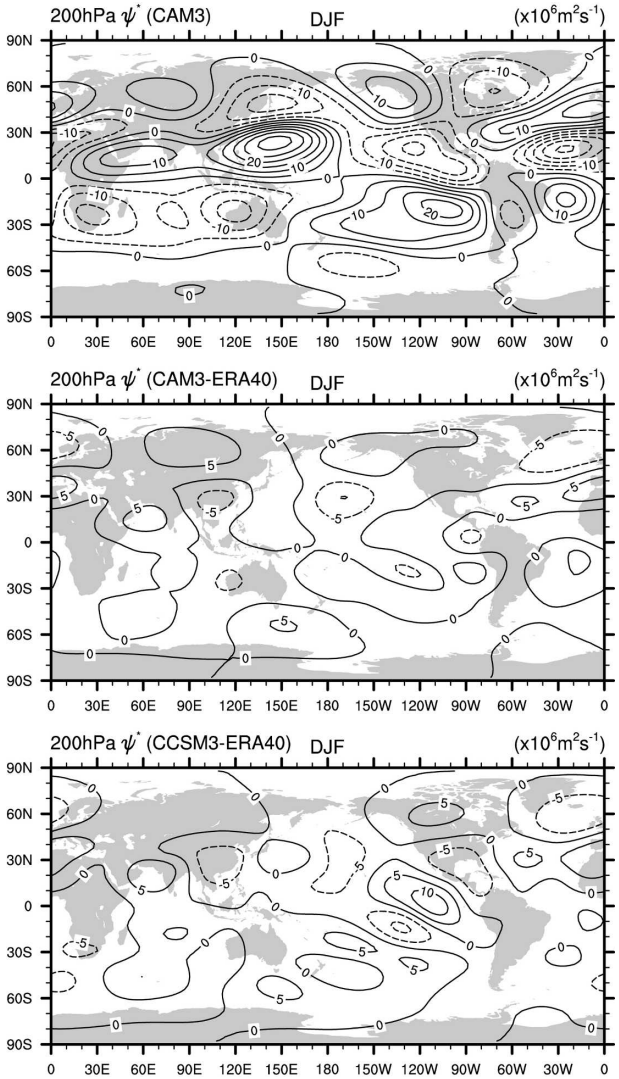

FIG. 10. (top) Mean DJF 200-hPa eddy streamfunction from CAM3, (middle) differences from the ERA-40 (1979–2000) climatology for CAM3, and (bottom) CCSM3. The contour increment is 5×10^6 m^2 s^{-1} and negative values are dashed.

over the Pacific Ocean, resulting in relatively weaker westerlies (the split jet) over New Zealand.

d. Rotational flow

The rotational component of the flow, as depicted by the streamfunction, is a well-measured quantity. Moreover, by examining departures from the zonal symmetry (i.e., the eddy streamfunction), stationary wave patterns extending through the Tropics can be examined. Regional differences between the simulated and observed eddy streamfunction at 200 hPa are shown in Figs. 10 and 11.

Early model versions exhibited significant errors in this field (Hurrell et al. 1993), but as for CCM3 the CAM3 simulates well the major circulation centers in the upper troposphere during both seasons. In particular, the low-latitude anticyclonic couplet over the tropical western Pacific is captured, although the centers over southern Africa and Australia are a bit too strong, consistent with the low- (high) latitude easterly (westerly) biases in those regions (Fig. 8). Over the central Pacific, the cyclonic couplet is well captured, although it is shifted to the east relative to observations (and CCM3), consistent with the low-latitude wind errors noted earlier. Recall, however, that these upper tropospheric wind errors are more pronounced in CCSM3, and this is evident in the eddy streamfunction plots. In particular, the cyclonic couplet is much weaker than observed and the NH center is shifted to the north in coupled simulation, resulting in the large easterly bias

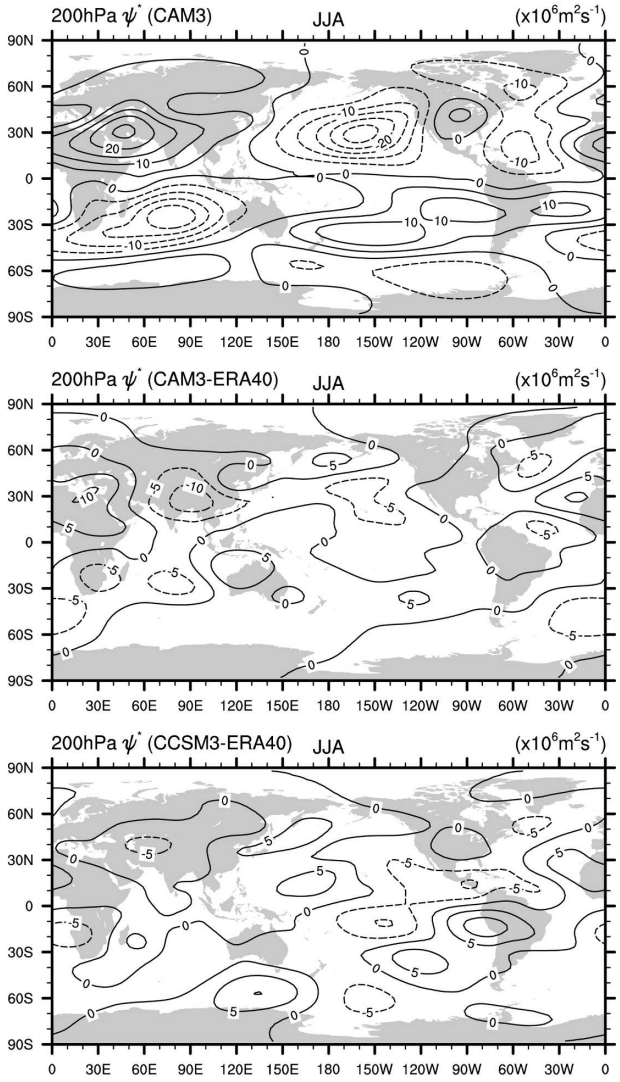

FIG. 11. As in Fig. 10 but for JJA.

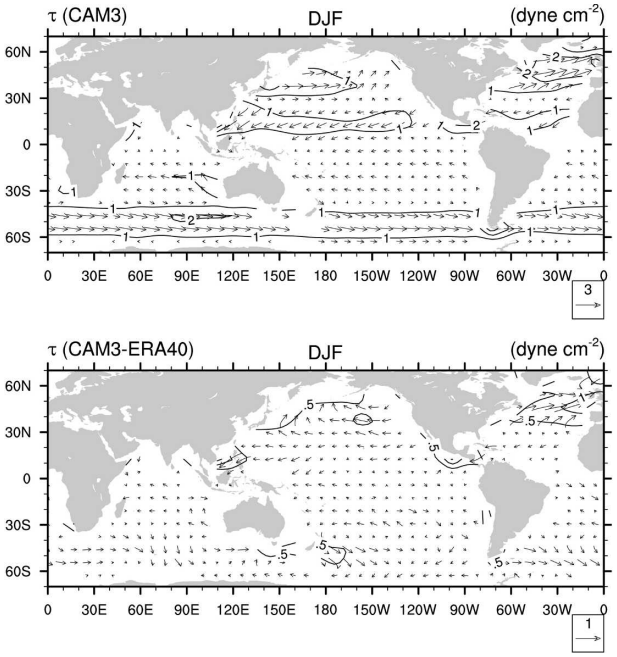

FIG. 12. (top) Mean DJF surface wind stress vectors from CAM3 and (bottom) differences from the ERA-40 (1979–2000) climatology. The magnitudes are contoured every 1 (0.5) dyn cm^{-2} in the top (bottom) panel, and the reference vector corresponds to 3.0 (1.0) dyn cm^{-2} in the top (bottom) panel.

just south of the equator near 125°W (Fig. 8). Over the tropical Atlantic, the cyclonic couplet is too strong in CAM3, especially in the SH, resulting in the 200-hPa equatorial westerly bias noted earlier.

During southern winter, the main features both observed and simulated by CAM3 include anticyclonic centers in the Eastern Hemisphere and subtropical troughs over the Pacific and Atlantic Oceans (Fig. 11). The zonal asymmetry is markedly smaller in the middle latitudes of the SH than at lower levels (not shown), although wave 1 is still evident. The cyclonic center east of New Zealand is simulated, so that the westerlies over New Zealand are at a relative minimum (Fig. 9), and the flow has a strong southerly component from the Indian Ocean across southern Australia. The most significant difference in CAM3 from observations during JJA arises from a slight westward shift and underestimate of the upper-level anticyclone associated with the summer monsoon circulation, which is consistent with the 200 hPa westerly bias over the tropical Indian Ocean. In CCSM3, the strong westerly bias in excess of 20 m s^{-1} over the equatorial eastern Pacific (Fig. 9) is associated with an erroneous cyclonic couplet centered over Central and South America (Fig. 11).

e. Surface wind stress

An important parameter for coupling AGCMs to dynamical ocean models is the surface wind stress (τ), by which the atmospheric winds drive the oceanic currents, and the ocean acts as a sink for atmospheric momentum. This field is a specified boundary condition in ocean general circulation models. The main biases in CAM3 relative to the climatological estimates from ERA-40 are consistent with errors in the SLP and near-surface wind fields (not shown).

The surface wind stress comparison (Figs. 12 and 13) indicates that the strength of the subtropical trade winds in CAM3 is too strong, consistent with higher than observed SLPs throughout the subtropics during both seasons (Figs. 1 and 2). This trade wind bias is very similar to that in CCSM3 (Large and Danabasoglu

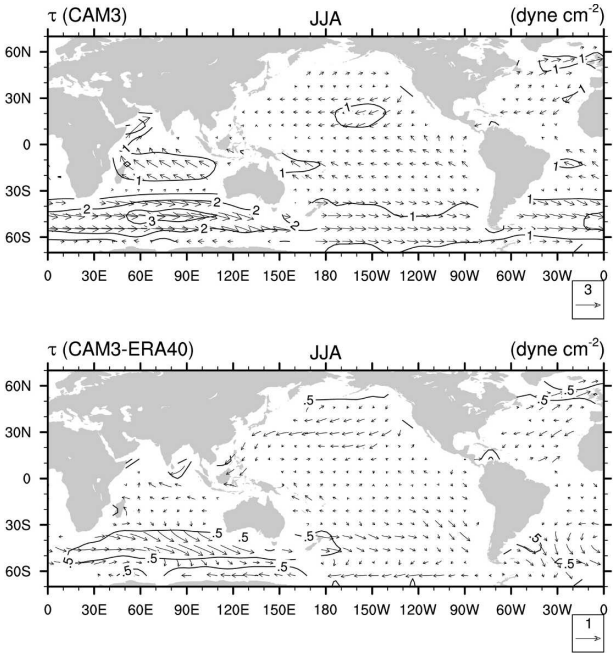

FIG. 13. As in Fig. 12 but for JJA.

2006), but smaller than in CCM3 (Hurrell et al. 1998). The difference vectors are of greatest magnitude over the extratropical oceans during winter, with particularly large westerly biases over the North Atlantic (Fig. 12) and the Southern Ocean, especially over the Eastern Hemisphere (Fig. 13). Over the extratropical North Pacific, notable wintertime errors in CCM3 (Hurrell et al. 1998) are not evident in CAM3, reflecting an improved representation of the Aleutian low.

Over the tropical oceans the surface wind stress biases are slight during both seasons, including a realistic simulation of the surface flow associated with the Asian monsoon circulation during boreal summer (Fig. 13). During the same season, when coupled within CCSM3 (not shown), the simulated surface stresses are a maximum near 55°S, in good agreement with the latitude of maximum wind stress in the ERA-40 data. However, they are too strong by more than 1 dyn cm^{-2} over much of the Southern Ocean including the South Atlantic. This latter local bias is not as pronounced in the uncoupled CAM3 (Fig. 13), although the maximum stresses are too far equatorward: the maximum in the zonally averaged mean zonal wind stress (not shown) spans 45°–50°S. Large and Danabasoglu (2006) give a more detailed discussion of the simulated surface wind stress field in both CAM3 and CCSM3, and they conclude that CAM3 produces a reasonable mean and seasonal cycle of wind forcing, in particular over the tropical Pacific. In contrast, they show that the seasonal cycle of surface winds in CCSM3 is relatively poor and, thus, is likely an example of coupled error growth.

f. Irrotational flow

The divergent (i.e., irrotational) component of the wind plays a much more prominent role in the Tropics than in higher latitudes. The analysis of observed divergence is sensitive to the initialization technique, to the numerical prediction model used for the data assimilation and, in particular, to the parameterizations of convection used in the assimilating model. While the magnitude of the analyzed divergent wind (or vertical motion) varies considerably among different global analyses, including the reanalyses, it is generally true that the patterns of divergence are more robust. For this reason, differences between CAM3 and ERA-40 should be viewed qualitatively.

To first order, the meridional circulation in the Tropics represents the direct response to diabatic heating. Seasonal plots of the zonal-mean meridional streamfunction simulated by CAM3 (Fig. 14) reveal a strong intensification and predominance of the winter Hadley cell in each hemisphere with mass fluxes over 160×10^9 kg s^{-1}. Qualitatively, CAM3 is in slightly better agreement with reanalysis estimates (not shown) than CCM3, which had the center of the simulated circulation too low near 700 hPa (Hurrell et al. 1998). Both CAM3 and CCM3 place the main centers of the Hadley cells near 10°N in DJF and 5°S in JJA, in good agreement with ERA-40 estimates. Similarly, the CAM3 mean divergent zonal circulation (Fig. 15) also demonstrates very good agreement with observational estimates (e.g., Trenberth et al. 2000). In particular, regions of strong rising (e.g., centered near 135°E in DJF and 90°E in JJA) and sinking (e.g., near 100°E in DJF and 20°E in JJA) motion agree well, as do the magnitudes (exceeding 80×10^9 kg s^{-1} in DJF and 120×10^9 kg s^{-1} in JJA) and the centers of the circulation.

g. Precipitation

Hack et al. (2006a) and Rasch et al. (2006) discuss the thermodynamic structure and hydrologic cycle of CAM3 in detail. However, since precipitation is the result of links among the moisture, thermodynamics, and dynamics, the basic features of the CAM3 horizontal distribution are described briefly below. Comparisons to CMAP estimates are shown, although comparisons were also made to climatologies computed from the Global Precipitation Climatology Project (GPCP) data. Differences between these two observational estimates are significant locally, which underscores the point that comparisons to CAM3 should be viewed as

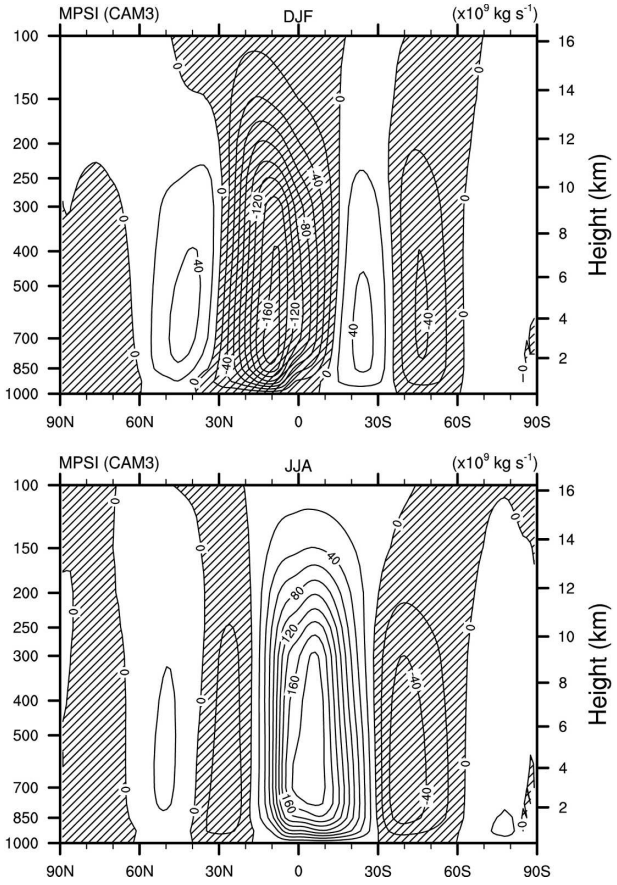

FIG. 14. Mean meridional streamfunction for (top) DJF and (bottom) JJA from CAM3. The contour increment is 20×10^9 kg s^{-1} and negative values are hatched.

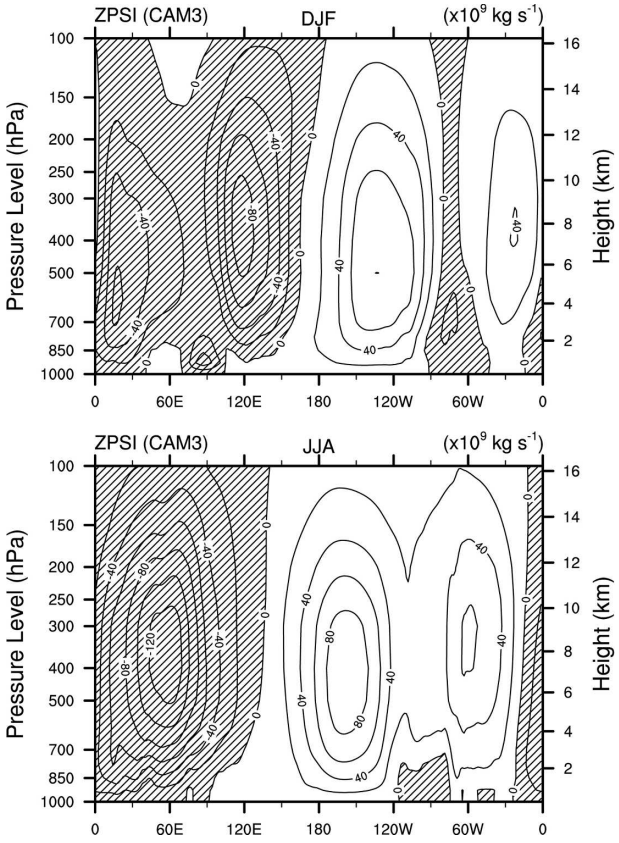

FIG. 15. Mean zonal streamfunction for (top) DJF and (bottom) JJA from CAM3. The contour increment is 20×10^9 kg s^{-1} and negative values are hatched.

qualitative. Nonetheless, biases are noted and assumed to be real when outside the range of observational estimates and physically consistent with previously mentioned errors in the dynamical simulation.

During DJF, large rainfall rates associated with convection in the South Pacific and South Atlantic convergence zones are captured by CAM3 and, as observed, they extend through the subtropics toward higher latitudes tapering to a minimum near 30°S (Fig. 16). Rainfall rates are much smaller during northern summer over these regions in both CAM3 and CMAP, when maximum rates occur near 10°N (Fig. 17). The low precipitation rates over the subtropics with minima over the eastern parts of the oceans of both hemispheres are well simulated by CAM3. In agreement with the CMAP estimates, secondary maxima in precipitation are simulated over middle latitudes during winter where polar fronts and their associated disturbances predominate. The more zonal orientation in the SH than in the NH broadly reflects the different patterns of cyclone frequency, although differences in the SH are more uncertain because of the lack of direct observations.

Although the CAM3 simulation captures many of the observed features in the global precipitation distribution, consistent with realistic patterns and magnitudes of low-level divergence and upper-level outflow (not shown), it continues to share many of the same biases exhibited by the CCM3 (Hack et al. 1998; Hurrell et al. 1998). For instance, there is a tendency for the simulated tropical precipitation maxima to remain in the NH throughout the year, while precipitation tends to be reduced along the equator relative to satellite estimates, particularly over the Indian Ocean. Most notable during northern winter are higher simulated rainfall rates just north of the equator near 150°E, over the eastern Pacific near 10°N, and over tropical Africa and the western Indian Ocean. Over the eastern Indian Ocean and the western Pacific, the zonally elongated maximum is just north of the equator, compared to near 5°S in the observational estimates. During JJA, CAM3 precipitation rates are unrealistically high over the western Indian Ocean and the Arabian Peninsula.

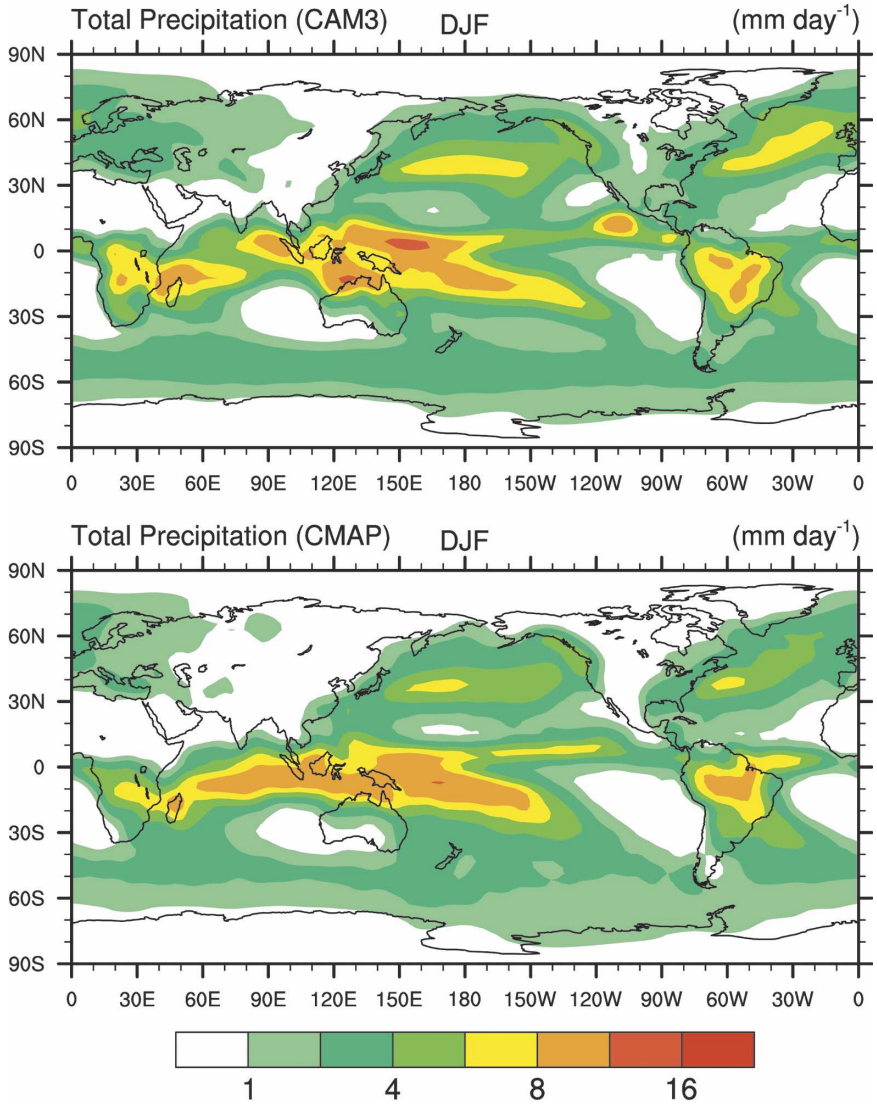

FIG. 16. Mean DJF total precipitation from (top) CAM3 and (bottom) the CMAP climatology. The contours are 1, 2, 4, 8, 12, and 16 mm day^{-1}.

Rainfall rates are too low from the South China Sea across the Philippine Sea, as well as within the Pacific and Atlantic ITCZ. Rainfall rates over the Caribbean Sea during JJA are too high, but are considerably smaller than in CCM3. Over the extratropics, the simulated precipitation is smaller than analyzed over the western boundary currents.

The horizontal distribution of precipitation in CCSM3 (not shown) is compared to that in CAM3 by Hack et al. (2006a). Briefly, the most notable changes occur over the tropical Pacific where coupling produces a significant and unrealistic enhancement in rainfall just south of the equator throughout the year, resulting in the so-called double ITCZ problem that plagues most coupled models. The tendency to produce a double ITCZ is also evident in the uncoupled simulation (Figs. 16 and 17), but it is much less pronounced. In contrast, coupling appears to improve the distribution of mean rainfall over Central America and the Caribbean, the western middle latitude boundary currents, the Arabian Peninsula, and the northern Indian Ocean.

h. Eddy statistics

A brief look at the eddy statistics of CAM3 is presented through plots of the transient eddy kinetic energy (EKE) $\frac{1}{2}(u'^2 + v'^2)$ and transient momentum flux $u'v'$. The distribution of these quantities in the upper troposphere indicates the ability of the CAM3 to depict the main storm tracks (e.g., Blackmon et al. 1977). All of the transient eddy statistics are based on daily data

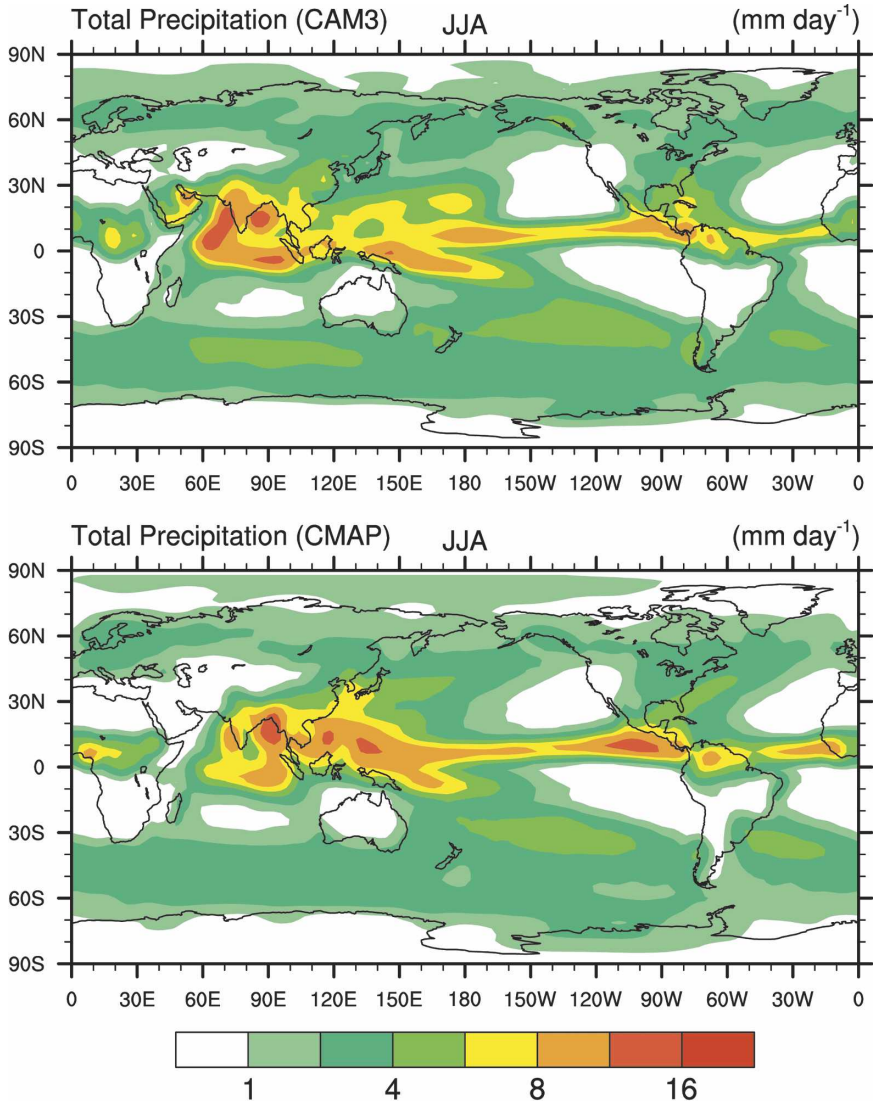

FIG. 17. As in Fig. 16 but for JJA.

that has been high-pass filtered to retain synoptic variations with periods of approximately 2–8 days.

Many of the general features and the interseasonal changes are well simulated by CAM3. Over the NH during winter, the CAM3 produces a belt of maximum EKE that extends from the Pacific across North America and the Atlantic into Europe (Fig. 18). During summer, the maximum values are weaker and shifted poleward of the wintertime belt by roughly 10° latitude (Fig. 19). The simulated maximum EKE over the SH encircles the globe between 40° and 50°S during austral summer, but during winter it shifts equatorward as observed, especially over the Pacific and Atlantic Oceans. Over both hemispheres, the belts of maximum EKE expand latitudinally during winter, reflecting the enhanced daily meandering of the polar and subtropical jet streams.

A primary difference from observations is that the synoptic variability in the extratropical storm tracks is generally overestimated by CAM3, which is opposite to the underestimation that characterized simulations with CCM3 (Hurrell et al. 1998). Only a small part of this difference can be explained by resolution: local 200-hPa EKE values in CAM3 simulations at T42 resolution (not shown) are within 10% of the values in Figs. 18 and 19 nearly everywhere. The largest increases in EKE due to better resolution of transient eddies with small meridional scales appear in the vicinity of the North Pacific jet in DJF and the subtropical jet over Australia in JJA.

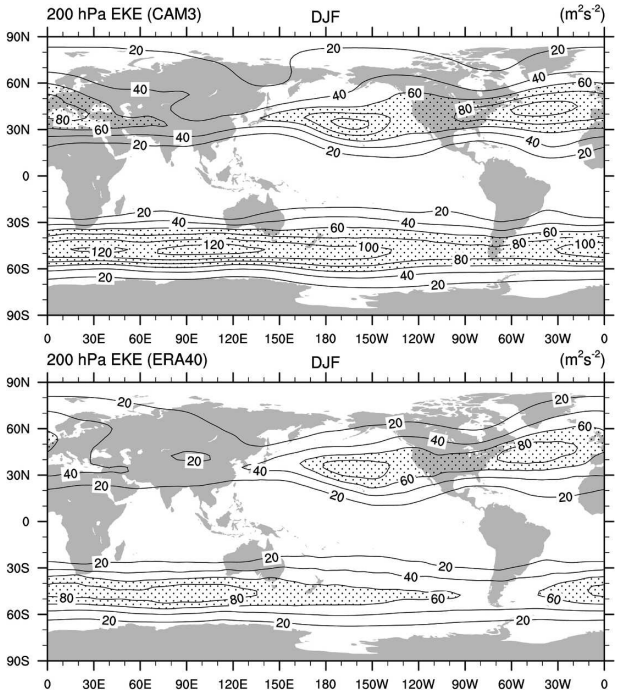

FIG. 18. Mean 200-hPa transient eddy kinetic energy (DJF) from (top) CAM3 and (bottom) ERA-40. The contour interval is 20 $m^2 s^{-2}$, and values greater than 60 $m^2 s^{-2}$ are stippled.

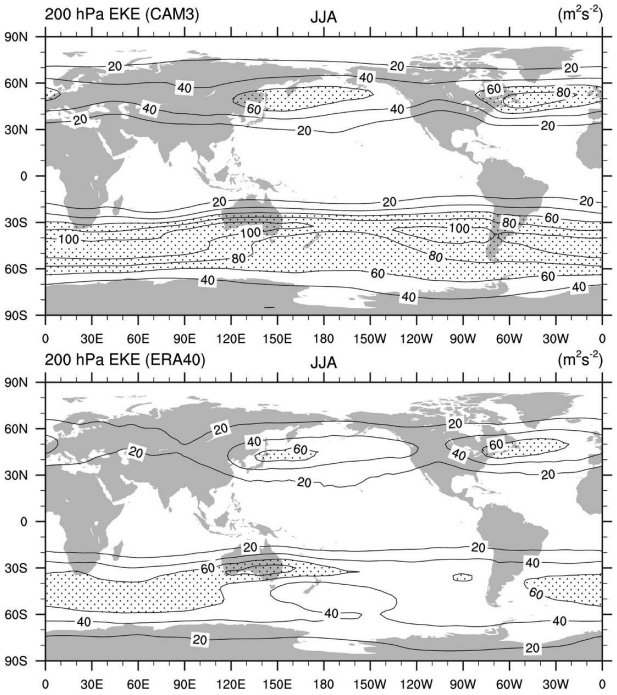

FIG. 19. As in Fig. 18 but for JJA.

Another general feature of the CAM3 storm tracks is that they tend to be zonally elongated relative to those in ERA-40, as was the case for CCM3. In particular, the CAM3 storm track does not tilt poleward across the North Atlantic in DJF as observed, consistent with mean zonal wind errors noted earlier (Fig. 8). The simulated SH storm track also tends to be more zonally symmetric than in ERA-40. For instance, during JJA the observed storm track spirals poleward over the Indian Ocean toward the Pacific resulting is a clear double maximum with minimum values over New Zealand. This minimum is present, but less pronounced in CAM3 (see also Fig. 9).

According to Eliassen and Palm (1961), the meridional propagation of transient eddies is proportional to and in the opposite direction of the transient momentum flux (Figs. 20 and 21). In general, CAM3 captures the overall structure and seasonal cycle well, although poleward $u'v'$ is overestimated in all regions and seasons except for the North Pacific during DJF and equatorward $u'v'$ is underestimated over the North Atlantic in DJF. Over the SH, the CAM3 transient momentum fluxes are much too strong throughout the year in all three ocean basins, and this error extends into the stratosphere, consistent with the westerly biases near 45°S in summer and 40°S in winter (Figs. 6 and 7). The excessive poleward momentum fluxes by synoptic eddies were also a feature of CCM3 and its predecessors (Hurrell et al. 1998).

i. Tropical intraseasonal oscillations

The tropical intraseasonal oscillation can be described, in simple terms, as a near-global scale, quasi-periodic, eastward-moving disturbance evident in tropospheric temperature and winds over the equatorial belt. The oscillation substantially modulates tropical convection, especially over the Indian and western Pacific Oceans, and, consequently, impacts the extratropics as well. A simple way of examining the tropical intraseasonal variability in an AGCM is to examine longitude–time plots of daily precipitation, outgoing longwave radiation, or upper-tropospheric winds or velocity potential near the equator. The latter variable, at 200 hPa averaged between 15°S and 15°N, is shown for December through May of one simulated year from CAM3 (Fig. 22, top panel). The values were obtained by first removing the mean (15 yr) annual cycle from each daily value, then filtering the daily data to remove fluctuations with periods less than about one week.

As with most AGCMs (e.g., Slingo et al. 1996; Sperber et al. 2004), including CCM3, the periodicity of the oscillation in CAM3 tends to be too short, nearer 20–30 days than 40–50 days as observed. Also, the observed phase speed is often faster over the Western Hemisphere (e.g., Weickmann and Khalsa 1990), a feature

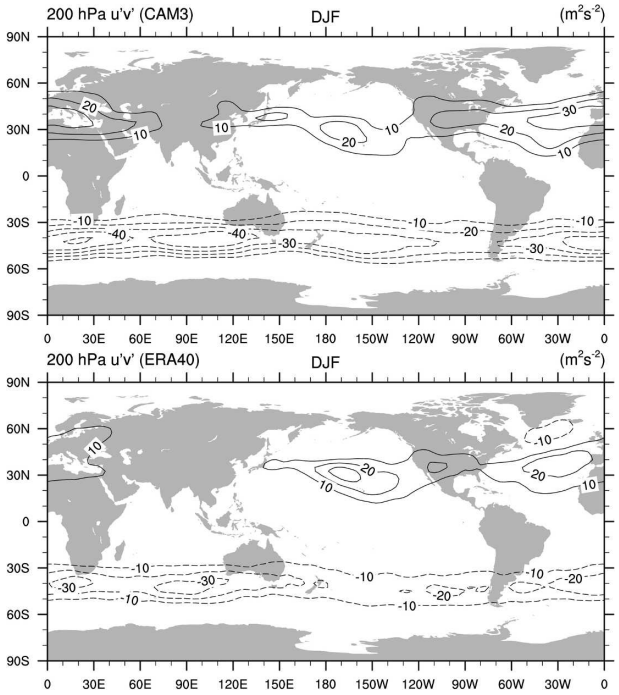

FIG. 20. Mean 200-hPa transient eddy meridional momentum flux (DJF) from (top) CAM3 and (bottom) ERA-40. The contour interval is 10 $m^2 s^{-2}$, negative contours are dashed, and the zero contour is omitted.

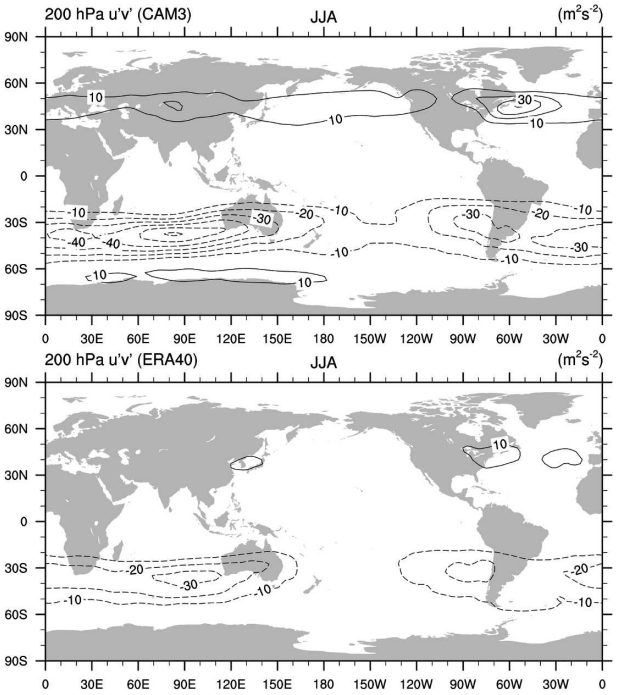

FIG. 21. As in Fig. 20 but for JJA.

not captured by CAM3. These aspects are more clearly illustrated through the time–longitude lag-correlation diagram in the lower panel of Fig. 22.

In general, tropical intraseasonal variability is not well simulated by CAM3, and its simulation is worse than in previous versions of the model. In particular, CAM3 considerably underestimates the amplitude of the oscillation relative to ERA-40 (not shown), and worse it is not evident in most simulated years (unlike CCM3). Moreover, the same can be said of CCSM3; thus, this shortcoming is not directly related to the absence of an interactive ocean (e.g., Waliser et al. 1999). The extent to which it is related to modifications of parameterized physical processes in CAM3 is a topic of ongoing investigation.

j. Tropical interannual variability

Over the Tropics there is a fairly direct tropospheric response to SST anomalies, and there is a large interannual signal associated with ENSO. Also, unlike the extratropics, masking by natural internal atmospheric variability is small. For these reasons, the model's ability to realistically mimic the observed atmospheric variability associated with ENSO is briefly examined. Deser et al. (2006) give a more detailed examination of the ENSO response in CAM3 (see also Hack et al. 2006a), and they also present an in-depth analysis of ENSO variability in CCSM3.

Observed shifts in tropical and subtropical convergence zones and seasonal rainfall anomalies associated with variations in ENSO are well simulated by CAM3 (Fig. 23), as they were by CCM3 (Hurrell et al. 1998; Hack et al. 1998). Shown is the observed and simulated rainfall as the difference from composites of warm and cold events since 1979 (when the CMAP record begins) during the boreal winter season. Warm and cold years were identified based on the criterion that the magnitude of the Niño-3.4 SST index (not shown) exceeds one standard deviation.

The observed distribution of tropical precipitation change is closely associated with the pattern of SST anomalies (not shown; see Figs. 6 and 8 of Deser et al. 2006). In particular, enhanced DJF precipitation in warm events is found over and near the region of positive SST anomalies in the eastern Pacific and western Indian Ocean, while reduced precipitation occurs over Indonesia, the South Pacific convergence zone (SPCZ) and the Atlantic ITCZ. The CAM3 precipitation composite clearly reflects most of these features. The main differences are that: 1) the negative anomalies in the SPCZ do not extend as far south as observed, 2) the negative anomalies over Indonesia and the eastern Indian Ocean are too weak, and 3) the simulated

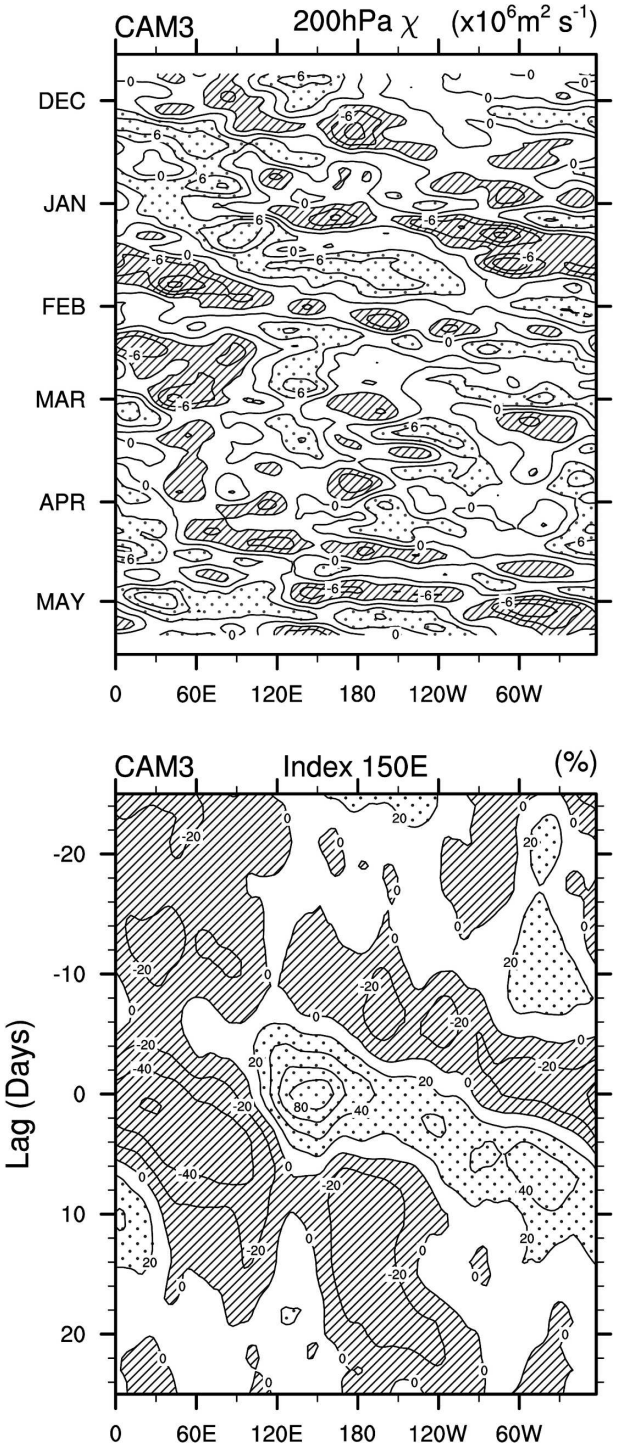

FIG. 22. (top) Time–longitude diagram (December–May) of the velocity potential at 200 hPa, averaged between 15°S and 15°N, from CAM. The contour increment is 3×10^6 m^2 s^{-1}, negative values are hatched, and positive values are stippled. (bottom) Lag correlations between an index of the tropical intraseasonal oscillation, given by the 200-hPa velocity potential averaged over the region 15°S–15°N, 140°–160°E, and the 200-hPa velocity potential at each longitude (averaged between 15°S and 15°N). The correlations are based on the daily values from December to May. The contour increment is 20%, negative correlations are hatched, and positive correlations are stippled.

precipitation response over the western Indian Ocean is mixed.

Relative to CCSM3 (not shown), the CAM3 simulation is much more realistic. As discussed in detail by Deser et al. (2006), the fully coupled simulation also exhibits enhanced rainfall in the vicinity of the equatorial Pacific SST warming, but the compensating regions of reduced rainfall occur preferentially to the north and south in a narrow equatorial zone rather than to the west over Indonesia as observed. These errors thus appear to be the consequence of deficiencies in the simulated CCSM3 ENSO SST signal rather than an intrinsic property of CAM3, although the precipitation response to ENSO in CAM3 is a bit more zonally oriented than in observations.

Examples of the dynamical response to interannual variations in tropical Pacific SSTs are given by the simulated and observed differences in the DJF mean divergent zonal circulation (Fig. 24) and 200-hPa eddy streamfunction (Fig. 25) between warm and cold event composites. The CAM3 simulation captures the shift in the main upward motion during DJF from being centered near 135°E in the climatological average (Fig. 15) to well east of the date line in warm events, although the strongest rising motion is a bit to the west of the ERA-40 estimates. The subsidence regions over South America and the western Pacific are also captured, although the latter is a bit weaker than observed consistent with the rainfall distributions (Fig. 23). Such changes in rainfall and, thus, the redistribution of latent heat release throughout the Tropics, drives an anomalous anticyclonic couplet over the tropical Pacific and a pattern that resembles the Pacific–North American teleconnection at higher latitudes, with anomalous cyclonic circulations over the Gulf of Alaska and the southeast United States (Fig. 25). Again, CAM3 captures the main features evident in the ERA-40 data, including the cyclonic couplet over the equatorial Atlantic. Deser et al. (2006) show similar maps, but for composite differences in SLP, surface air temperature, precipitation, and 500-hPa geopotential height for both DJF and JJA. From this more comprehensive evaluation, they also conclude the CAM3 response to ENSO variability is quite realistic.

k. Extratropical modes of variability

In addition to ENSO, a very large fraction of large-scale atmospheric variability can be attributed to two other principal patterns (or modes) of variability (Quadrelli and Wallace 2004; Trenberth et al. 2005): the Northern and Southern Annular Modes, known as the NAM and the SAM, respectively (e.g., Thompson and Wallace 2000). The NAM is defined as the first empiri-

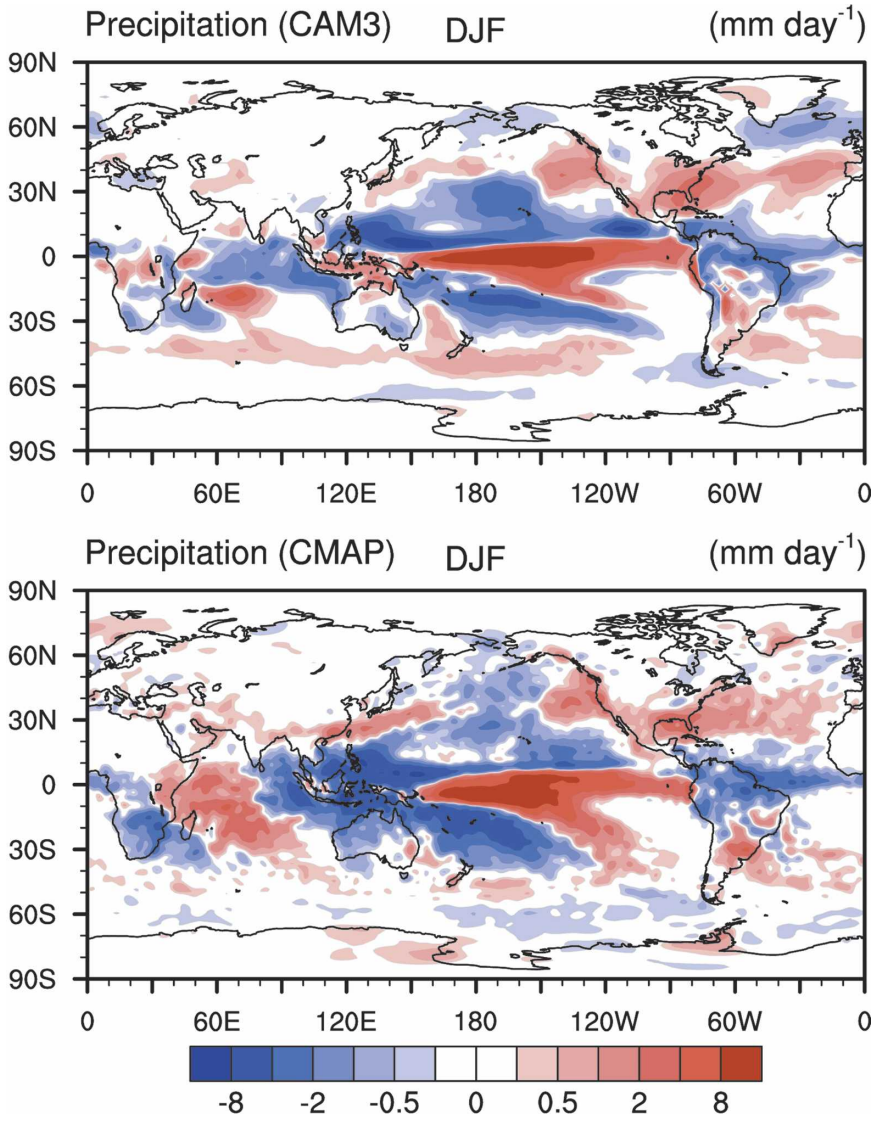

FIG. 23. Warm–cold ENSO event anomaly composites of precipitation during DJF for (top) CAM3 and (bottom) CMAP. The contours are ± 0.25, 0.5, 1, 2, 4, and 8 mm day^{-1}.

cal orthogonal function (EOF) of NH (20°–90°N) winter SLP data. Following Thompson et al. (2003), the SAM is defined as the leading EOF of the SH (90°–20°S) monthly mean 700-hPa height field (to partially alleviate ambiguities introduced by the reduction to sea level over the high terrain of Antarctica). The patterns are displayed in terms of amplitude, obtained by regressing the hemispheric anomalies upon the leading principal component time series (Figs. 26 and 27). The basic structures of both the NAM and the SAM arise from the internal, nonlinear dynamics of the atmosphere; thus, the patterns presented here do not differ significantly from those obtained from CAM3 simulations forced with climatological annual cycles (no interannual variations) of all forcings external to the atmosphere (not shown).

The NAM and SAM patterns in ERA-40 data are both predominantly zonally symmetric (the SH pattern somewhat more so), and both exhibit similar amplitudes and meridional scales that reflect a seesaw in lower tropospheric heights between polar and middle latitudes. As noted by Deser (2000), Wallace (2000), Hurrell et al. (2003), and Thompson et al. (2003) among several others, the NAM is virtually identical to the leading EOF of the Euro-Atlantic sector: the well-known North Atlantic Oscillation (NAO). Both the NAM and the NAO have a strong zonally symmetric component, but the hemispheric EOF has

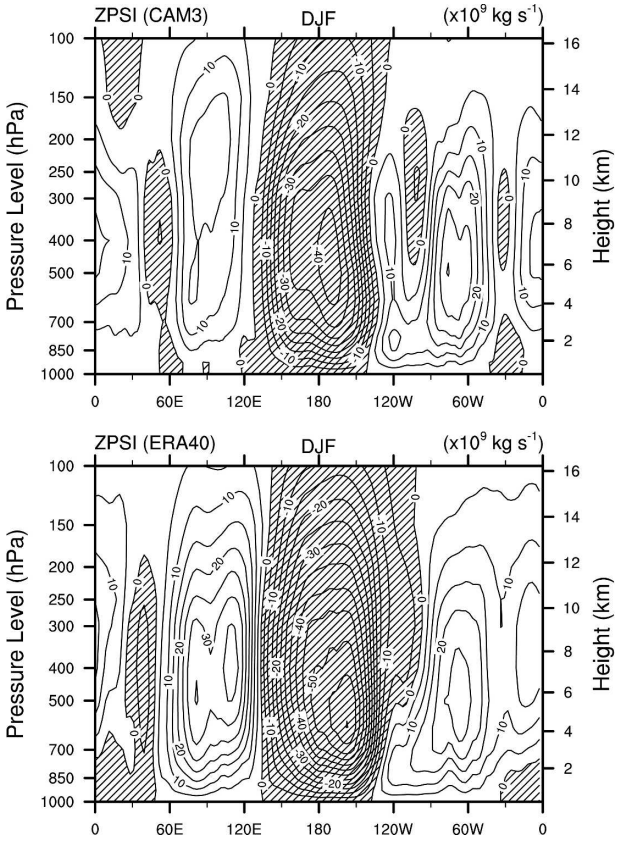

FIG. 24. Warm–cold ENSO event anomaly composites of mean zonal streamfunction during DJF for (top) CAM3 and (bottom) ERA-40. The contour increment is 5×10^9 kg s^{-1} and negative values are hatched.

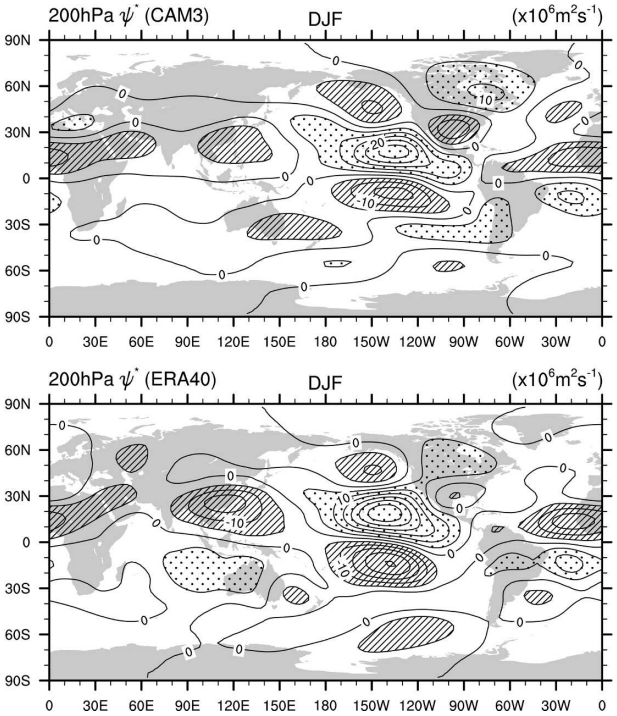

FIG. 25. Warm–cold ENSO event anomaly composites of 200-hPa eddy streamfunction for (top) CAM3 and (bottom) ERA-40. The contour increment is 5×10^6 m^2 s^{-1}, values less than -5×10^6 m^2 s^{-1} are hatched, and values greater than 5×10^6 m^2 s^{-1} are stippled.

slightly larger amplitudes (~0.5 hPa) over the Pacific sector.

The leading hemispheric EOFs in the CAM3 simulation bear a strong resemblance to the observed NAM and SAM structures, yet several differences are notable. In particular, the simulated NAM exhibits larger amplitudes, especially over the North Pacific, the polar center is too expansive, and the Atlantic centers of action are shifted to the east. This latter error is consistent with biases in the mean Atlantic SLP, winds and storm tracks noted earlier, especially that the simulated Icelandic low is too deep and it extends too far to the east (Fig. 1). The dynamical signature of interannual variability can also be examined by nonlinear approaches, such as cluster analysis or nonlinear principal component analysis. Alexander et al. (2006) applied the former to CCSM3 simulations, and their first two winter regimes over the North Atlantic captured the positive and negative phases of the NAO. Moreover, both regimes exhibited the same biases evident in Fig. 26, which suggests they are mainly due to the atmosphere and not air–sea coupling. Over the extratropical SH, the amplitude of the simulated SAM is much closer to that observed, and the overall spatial structure is well captured.

5. Summary

Climate system models are needed to understand and consider simultaneously the wide range of complex interacting physical, chemical, and biological processes that characterize the atmosphere, ocean, and land. Before simulations from models such as CCSM3 can be fully comprehended, however, it is necessary to understand the strengths and weaknesses of the component models. This paper summarizes the dynamical aspects of simulations with the latest version of the Community Atmosphere Model, CAM3.

The most important differences from the previous version of the model, CCM3, are associated with changes to the parameterized physics package. These changes have resulted in a modest improvement in the overall simulated climate of the model. At sea level, the model reproduces the basic observed patterns of the pressure field quite well, including the major intersea-

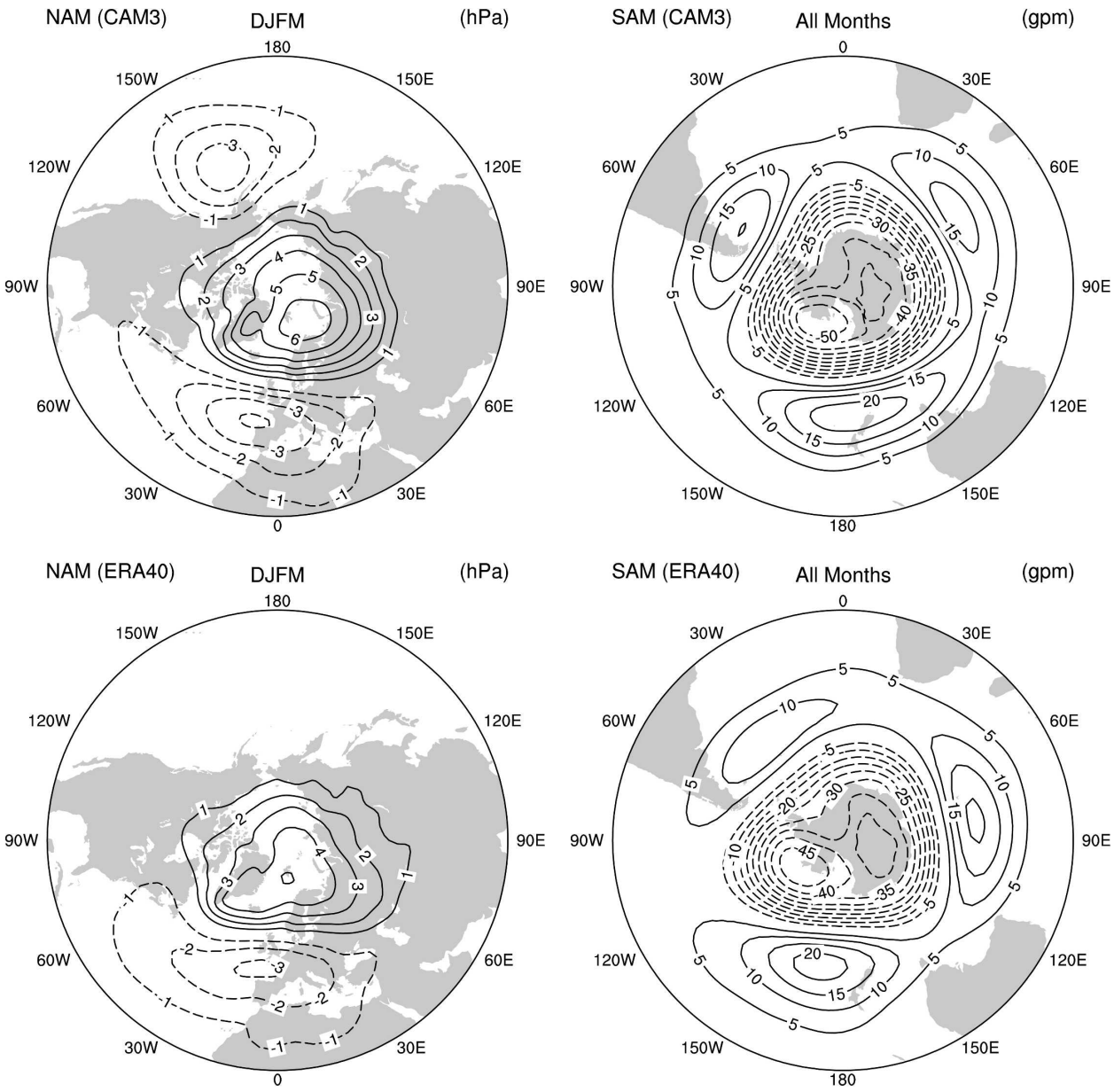

FIG. 26. Leading empirical orthogonal function of the winter (December–March) mean sea level pressure anomalies over the Northern Hemisphere (20°–90°N) for (top) CAM3 and (bottom) ERA-40. The patterns are displayed in terms of amplitude (hPa), obtained by regressing the hemispheric sea level pressure anomalies upon the leading principal component time series. The contour interval is 1 hPa, the zero line is omitted, and negative contours are dashed.

FIG. 27. Leading empirical orthogonal function of the monthly mean 700-hPa geopotential height anomalies over the Southern Hemisphere (90°–20°S) for (top) CAM3 and (bottom) ERA-40. The patterns are displayed in terms of amplitude (m), obtained by regressing the hemispheric height anomalies upon the leading principal component time series. The contour interval is 5 m, the zero line is omitted, and negative contours are dashed.

sonal changes in the subtropical high pressure centers and the higher-latitude low pressure systems. The SLP distribution throughout the subtropics of both hemispheres is higher than observed during DJF and JJA, however, whereas pressures in subpolar latitudes tend to be too low. The largest regional differences are similar to those observed in CCM3. In particular, SLP differences over the NH occur where the simulated highs over the eastern Pacific and Atlantic Oceans are too strong during boreal winter, and erroneously low pressures at higher latitudes are most notable over Europe and Eurasia. Over the SH, the circumpolar Antarctic trough is too deep throughout the year, and the largest

differences are found south of New Zealand where the model fails to capture the observed weakening and poleward shift of the maximum meridional pressure gradient.

The simulation of the middle-tropospheric flow is very good in CAM3, with regional differences from observations broadly consistent with the biases evident in the simulated SLP. The model successfully reproduces the observed large-scale zonal asymmetries at 500 hPa, including the dominance of wavenumber 1 at high latitudes of the SH throughout the year, and the very large interseasonal changes in the quasi-stationary wave structure over the NH. The major shortcoming of the simulation is that CAM3 500-hPa heights are higher than observed throughout the Tropics and subtropics, consistent with a slight warm bias in the tropical troposphere (Hack et al. 2006a).

The zonal wind structure in CAM3 is close to that observed, although the middle-latitude westerlies are too strong in both hemispheres throughout the year. These westerly biases, which are consistent with errors in the pressure fields and the simulated transient momentum fluxes, are largest during northern summer and exceed 8 $m\,s^{-1}$ in the zonal-mean upper-tropospheric flow over both the NH and the SH. An overall view of the upper-tropospheric flow, as measured by the horizontal streamfunction, reveals that the major circulation centers and their interseasonal changes are very well simulated by the model, both in terms of magnitude and location. Closer to the surface, the CAM3 trade winds are in good agreement with ERA-40 data, although a bit too strong, which is consistent with the enhanced subtropical high pressure centers in the model. This error leads to a slight easterly bias in the simulated surface wind stress.

The observed patterns and magnitudes of upper-level divergent outflow are well simulated by CAM3, a finding consistent with an improved and overall realistic simulation of tropical precipitation. During northern winter, the CAM3 simulates the observed maxima in precipitation associated with the convergence zones over the South Pacific, South America, and Africa. Rainfall rates over the latter region are higher than observed, however, as are rates over the western Indian Ocean. In general, there is a tendency for the simulated tropical precipitation maxima to remain in the NH throughout the year, while precipitation tends to be less than indicated by satellite estimates along the equator. During JJA, precipitation rates are unrealistically high over the western Indian Ocean and the Arabian Peninsula, while they are too low within the Pacific and Atlantic ITCZ and from the South China Sea across the Philippine Sea.

While our focus has been on the simulation of the mean state, the simulated interannual variability of the CCM3 compares well to observations. For example, well-known changes in tropical and subtropical precipitation related to ENSO, together with associated anomalous wave trains that extend into extratropical latitudes, are well simulated by the model. Similarly, principal modes of extratropical variability bear considerable resemblance to those observed, although biases in the mean state over the North Atlantic degrade the simulated structure of the leading mode of atmospheric variability over the NH. In contrast, tropical intraseasonal variability is not well simulated by CAM3, and its simulation is worse than in previous versions of the model.

Comparison studies are only one approach to improve our understanding of the way models and the climate system operate. Given the enormous complexity of AGCMs, the simple identification of differences from observations does not easily translate into model improvements. Moreover, many other important aspects of the ability of the CAM3 to simulate the observed climate were not presented in this paper, but they are described elsewhere in this special issue. Other focused activities, such as hypothesis-driven numerical experiments, will help achieve further progress on understanding the physical reasons behind the major simulation deficiencies that remain in the latest version of the Community Atmosphere Model.

Acknowledgments. This study is based on model integrations performed by NCAR and CRIEPI with support and facilities provided by NSF, DOE, MEXT, and ESC/JAMSTEC. We thank the two anonymous referees whose comments helped to improve the paper.

REFERENCES

Alexander, M., and Coauthors, 2006: Extratropical atmosphere–ocean variability in CCSM3. *J. Climate,* **19,** 2492–2521.

Blackmon, M. L., J. M. Wallace, N.-C. Lau, and S. L. Mullen, 1977: An observational study of the Northern Hemisphere wintertime circulation. *J. Atmos. Sci.,* **34,** 1040–1053.

Boville, B. A., P. J. Rasch, J. J. Hack, and J. R. McCaa, 2006: Representation of clouds and precipitation processes in the Community Atmosphere Model version 3 (CAM3). *J. Climate,* **19,** 2162–2183.

Collins, W. D., and Coauthors, 2004: Description of the NCAR Community Atmosphere Model (CAM3). Tech. Rep. NCAR/TN-464+STR, National Center for Atmospheric Research, Boulder, CO, 226 pp.

——, and Coauthors, 2006a: The Community Climate System Model version 3 (CCSM3). *J. Climate,* **19,** 2122–2143.

——, and Coauthors, 2006b: The formulation and atmospheric simulation of the Community Atmosphere Model version 3 (CAM3). *J. Climate,* **19,** 2144–2161.

Deser, C., 2000: On the teleconnectivity of the Arctic Oscillation. *Geophys. Res. Lett.,* **27,** 779–782.

——, A. Capotondi, R. Saravanan, and A. Phillips, 2006: Tropical Pacific and Atlantic climate variability in CCSM3. *J. Climate,* **19,** 2451–2481.

DeWeaver, E., and C. M. Bitz, 2006: Atmospheric circulation and its effect on Arctic sea ice in CCSM3 simulations at medium and high resolutions. *J. Climate,* **19,** 2415–2436.

Eliassen, A., and E. Palm, 1961: On the transfer of energy in stationary mountain waves. *Geofys. Publ.,* **22** (3), 1–23.

Fiorino, M., 2004: A multi-decadal daily sea surface temperature and sea ice concentration data set for the ERA-40 reanalysis. ERA-40 Project Report Series 12, 16 pp.

Gates, W. L., and Coauthors, 1999: An overview of the results of the Atmospheric Model Intercomparison Project (AMIP I). *Bull. Amer. Meteor. Soc.,* **80,** 335–345.

Hack, J. J., J. T. Kiehl, and J. W. Hurrell, 1998: The hydrologic and thermodynamic characteristics of the NCAR CCM3. *J. Climate,* **11,** 1179–1206.

——, J. M. Caron, S. G. Yeager, K. W. Oleson, M. M. Holland, J. E. Truesdale, and P. J. Rasch, 2006a: Simulation of the global hydrological cycle in the CCSM Community Atmosphere Model version 3 (CAM3): Mean features. *J. Climate,* **19,** 2199–2221.

——, ——, G. Danabasoglu, K. Oleson, and C. Bitz, 2006b: CCSM3–CAM3 climate simulation sensitivity to increased horizontal resolution. *J. Climate,* **19,** 2267–2289.

Hurrell, J. W., J. J. Hack, and D. P. Baumhefner, 1993: Comparison of NCAR Community Climate Model (CCM) climates. NCAR Tech. Note NCAR/TN-395+STR, 335 pp.

——, ——, B. A. Boville, D. L. Williamson, and J. T. Kiehl, 1998: The dynamical simulation of the NCAR Community Climate Model Version 3 (CCM3). *J. Climate,* **11,** 1207–1236.

——, Y. Kushnir, G. Ottersen, and M. Visbeck, 2003: An overview of the North Atlantic Oscillation. *The North Atlantic Oscillation: Climatic Significance and Environmental Impact, Geophys. Monogr.,* No. 134, Amer. Geophys. Union, 1–35.

Kiehl, J. T., J. J. Hack, G. B. Bonan, B. A. Boville, D. L. Williamson, and P. J. Rasch, 1998: The National Center for Atmospheric Research Community Climate Model: CCM3. *J. Climate,* **11,** 1131–1149.

Large, W. G., and G. Danabasoglu, 2006: Attribution and impacts of upper-ocean biases in CCSM3. *J. Climate,* **19,** 2325–2346.

Oleson, K. W., and Coauthors, 2004: Technical description of the Community Land Model (CLM). Tech. Rep. NCAR/TN-461+STR, National Center for Atmospheric Research, Boulder, CO, 174 pp.

Quadrelli, R., and J. M. Wallace, 2004: A simplified linear framework for interpreting patterns of Northern Hemisphere wintertime climate variability. *J. Climate,* **17,** 3728–3744.

Raphael, M., 1998: Quasi-stationary waves in the Southern Hemisphere: An examination of their simulation by the NCAR Climate System Model, with and without an interactive ocean. *J. Climate,* **11,** 1405–1418.

Rasch, P. J., and Coauthors, 2006: Characterization of tropical transient activity in the CAM3 atmospheric hydrologic cycle. *J. Climate,* **19,** 2222–2242.

Rayner, N. A., D. E. Parker, E. B. Horton, C. K. Folland, L. V. Alexander, and D. P. Rowell, 2003: Global analyses of SST, sea ice and night marine air temperature since the late nineteenth century. *J. Geophys. Res.,* **108,** 4407, doi:10.1029/2002JD002670.

Reynolds, R. W., N. A. Rayner, T. M. Smith, D. C. Stokes, and W. Wang, 2002: An improved in situ and satellite SST analysis for climate. *J. Climate,* **15,** 1609–1625.

Slingo, J. M., and Coauthors, 1996: Intraseasonal oscillations in 15 atmospheric general circulation models: Results from an AMIP diagnostic subproject. *Climate Dyn.,* **12,** 325–357.

Sperber, K. R., J. M. Slingo, P. M. Inness, S. Gualdi, W. Li, P. J. Gleckler, and C. Doutriaux, 2004: The Madden–Julian Oscillation in GCMs. *Proc. Second Phase of the Atmosphere Model Intercomparison Project (AMIP2): Toward Innovative Model Diagnostics,* Toulouse, France, 81–85.

Taylor, K. E., D. Williamson, and F. Zwiers, 2000: The sea surface temperature and sea-ice concentration boundary conditions of AMIP II simulations. PCMDI Rep. 60, 20 pp.

Thompson, D. W. J., and J. M. Wallace, 2000: Annular modes in the extratropical circulation. Part I: Month-to-month variability. *J. Climate,* **13,** 1000–1016.

——, S. Lee, and M. P. Baldwin, 2003: Atmospheric processes governing the Northern Hemisphere Annular Mode/North Atlantic Oscillation. *The North Atlantic Oscillation: Climatic Significance and Environmental Impact, Geophys. Monogr.,* No. 134, Amer. Geophys. Union, 81–112.

Trenberth, K. E., D. P. Stepaniak, and J. M. Caron, 2000: The global monsoon as seen through the divergent atmospheric circulation. *J. Climate,* **13,** 3969–3993.

——, ——, and L. Smith, 2005: Interannual variability of patterns of atmospheric mass distribution. *J. Climate,* **18,** 2812–2825.

van Loon, H., 1972: Temperature, pressure, wind, cloudiness and precipitation in the Southern Hemisphere. *Meteorology of the Southern Hemisphere, Meteor. Monogr.,* No. 35, Amer. Meteor. Soc., 25–111.

Waliser, D. E., K. M. Lau, and J.-H. Kim, 1999: The influence of coupled sea surface temperatures on the Madden–Julian oscillation: A model perturbation experiment. *J. Atmos. Sci.,* **56,** 333–358.

Wallace, J. M., 2000: North Atlantic Oscillation/annular mode. Two paradigms—one phenomenon. *Quart. J. Roy. Meteor. Soc.,* **126,** 791–805.

Weickmann, K. M., and S. J. S. Khalsa, 1990: The shift of convection from the Indian Ocean to the western Pacific Ocean during a 30–60 day oscillation. *Mon. Wea. Rev.,* **118,** 964–978.

Xie, P., and P. A. Arkin, 1996: Analyses of global monthly precipitation using gauge observations, satellite estimates, and numerical model predictions. *J. Climate,* **9,** 840–858.

Yeager, S. G., C. A. Shields, W. G. Large, and J. J. Hack, 2006: The low-resolution CCSM3. *J. Climate,* **19,** 2545–2566.